

Investigating the Effect of GNP Addition on Self-healing of ECC through Mechanical and Nondestructive Testing

Aysu Göçügenci^{1*}, Süleyman Bahadır Keskin¹

¹ Department of Civil Engineering, Faculty of Engineering, Muğla Sıtkı Koçman University, 43/25 Marmaris Yolu Blv., 48050 Menteşe, Muğla, Türkiye

* Corresponding author, e-mail: aysugocugenci@mu.edu.tr

Received: 06 July 2023, Accepted: 07 December 2023, Published online: 20 February 2024

Abstract

Inclusion of nanomaterials is an effective method for enhancing the mechanical and durability characteristics of cement-based materials. Among various graphene-based nanomaterials, graphene nanoplatelets (GNPs) are cost-effective nanoparticles that possess graphene's key properties. Since limited information is available regarding their influence on the fresh, mechanical, non-destructive, and self-healing behavior of Engineered Cementitious Composites (ECC), this research focuses on GNP inclusion on these properties of ECC in a comprehensive way. In this research, the changes in material properties of ECC were monitored with several mechanical and nondestructive test methods. According to the results, GNP inclusion significantly enhanced flexural behavior and also promoted self-healing of ECC, with preloaded specimens exhibiting substantial or complete crack closure and similar performance to virgin specimens. Non-destructive tests and microstructural analyses also confirmed the promoting effects of GNP. A noticeable increase was observed in compressive strength when GNP was included. In conclusion, this study provides compelling evidence about the positive impact of GNP inclusion on improving the properties of ECC. The findings demonstrate the potential of GNPs to enhance the performance of cementitious materials and offer valuable insights for future research and practical applications.

Keywords

graphene nanoplatelets, engineered cementitious composites, self-healing, nanomaterials, nondestructive testing

1 Introduction

The demand for high-performance construction materials has been steadily increasing due to the growing need to construct more resilient and sustainable structures. The primary focus of this development is typically on enhancing the various properties of cementitious materials including the mechanical and durability behaviors. Despite their widespread usage in many structural applications, cementitious materials are intrinsically brittle and have low tensile strength. Utilizing fibers as reinforcement is an effective approach for enhancing the ductility and tensile characteristics of cementitious materials. Ultra-high performance fiber reinforced cementitious composites (UHPRCC) are able to present high levels of tensile ductility due to the presence of fibers. Engineered cementitious composites (ECC) are micro-mechanically tailored, unique type of UHPRCC that incorporate polyvinyl alcohol (PVA) fibers in their mix design. ECC exhibits tensile ductility and tensile strain capacity up to 3 or 5% which are significantly higher than traditional concrete and also

fiber-reinforced concrete, exceeding them by several hundred times [1]. Due to the presence of 2% by volume PVA fibers and mix proportions, this material is able to show strain hardening and multiple cracking behavior under the tensile effect. A microcrack initiates from a defect point and remains flat, whereas fibers resist and transfer the load by functioning as a bridge without rupture. As the load increases, additional microcracks start from other defect points and propagate without widening, resulting in the steady-state multiple micro-cracking behavior of ECC [2]. After the first crack formation, ECC exhibits an ability to withstand increasing loads and undergo significant deformations through multiple cracking. This strain-hardening behavior enhances the material's ductility and toughness. The interaction between fiber and matrix controls the crack propagation dynamics of ECC as well. The multiple cracking and strain hardening behaviors consequently induce microcracks with tight crack widths below 100 μm [3]. Incorporating nanomaterials, such as silica, nano-alumina,

titanium dioxide nanoparticles, and carbon based nanotubes, nanofibers, graphene, its oxides and nanoplatelets is also an efficient approach to modify the mechanical and durability characteristics of cementitious materials [4, 5]. Compared to other graphene-based materials, graphene nanoplatelets (GNPs) are cost-efficient nanoparticles [6]. The structure of GNPs consists of two-dimensional sheets that are less than 10 nanometers in thickness. GNPs possess the fundamental features of graphene due to their composition of graphene stacks in their crystallographic configuration [7, 8]. However, GNP studies report that GNPs tend to agglomerate in water due to their hydrophobic nature, hindering their widespread utilization in cement-based composites [9]. Therefore, it is important to disperse and stabilize GNPs before use. The dispersion of GNP also plays a crucial role in the material behavior as well-dispersed GNPs have an enhancing impact at low contents while agglomerated GNPs have a weakening impact at high contents, on material properties [10]. The distribution of GNPs into the matrix can be achieved by either a dry or wet process. Dry dispersion involves the direct mixing of GNPs with cement, followed by mechanical stirring [11]. In wet dispersion, the mechanical stirring of GNPs in water with surfactant is provided. As the GNPs in water with polycarboxylate-based superplasticizer are mixed via high shear mixing in combination with ultrasonication, it results in smaller graphene sheets and uniform dispersion. Ultrasonication or ultrasonic treatment can be achieved by using either a probe or an ultrasonic bath. During the treatment process, ultrasonication creates cavitation micro-bubbles which collapse quickly and form shockwaves that help to dissolve GNP agglomerates [12]. The incorporation of polycarboxylate-based superplasticizers as a surfactant effectively improves the stability and dispersion of GNPs in water [13]. Several studies in the literature revealed that once dispersed uniformly, GNPs improve especially mechanical and durability properties of cement-based materials. In a study by Du and Pang [4] on the transport properties of mortars containing GNP, the addition of 2.5% GNP stabilized by using the wet dispersion with ultrasonic treatment and a surfactant usage resulted in a decrease in permeability, water penetration, chloride diffusion and migration coefficients, without substantial improvement in mechanical properties. Tong et al. [8] studied the durability-related performance of graphene-reinforced mortar by applying wet dispersion, ultrasonic treatment, and water-reducing admixture usage. It was found that even small percentages of GNPs and

graphene oxide nanoplatelets (GONPs) increased compressive strength and improve resistance to chemical attack and corrosion. GNPs limited freeze-thaw performance, but GONPs improved it. The effects of GNPs and GONPs on strength, electrical resistance, and piezo-resistive reactions of mortar specimens were investigated by Liu et al. [7]. Through wet dispersion with ultrasonic treatment and surfactant usage, small percentages of GNPs and GONPs improved the concrete strength and reduced the penetration depth. GNPs are superior alternatives for usage as a conductive filler. According to Wang and Shuang [14], 0.05% GNP content wet-dispersed with ultrasonication had an optimum reinforcing effect on cement composites by increasing the compressive and flexural strength. GNPs were demonstrated to decrease porosity, median pore diameter, average pore diameter and affect larger pores by reducing them into smaller pores, leading to a refined and compact pore structure. The effects of GNP addition on freeze-thaw (F-T) resistance of concrete were also studied [15]. GNP concrete presented a finer pore structure with reduced workability. The highest compressive strength was found in specimens with 0.05% GNP. During freezing-thawing, concrete containing 0.05% GNP lost less mass and showed a better F-T resistance. As the impact of GNPs on hydration reactions, mechanical properties, and microstructure of cement composites were examined [16], it was discovered that 0.06% GNP used by wet dispersion, probe ultrasonication with superplasticizer increased the compressive and flexural strength, optimized the pore structure, decreased average pore diameter and porosity. Jiang et al. [12] analyzed the effects of dispersion techniques and amounts of GNPs on mechanical properties. The most efficient technique was high shear mixing alone or with ultrasonication and polycarboxylate-based superplasticizers. For compressive strength, low dosages of GNPs resulted in improvement, higher dosages in decrement due to agglomeration and no significant impact on flexural strength at any concentration. When subjected to chloride ion corrosion, microstructure and compressive properties of concrete were evaluated to observe the effects of 0.05% graphene nanoplatelets through direct mixing [17]. Results showed that the deterioration of concrete was prevented, and compressive strength and chloride resistance was improved with GNP usage. Zhang et al. [18] explored the impacts of 0.05% GNP on concrete carbonation depth in exposure to diverse climate conditions like varying temperature, CO₂ concentration and relative humidity. Within defined limits of these conditions, GNP

delayed the carbonation and increased the carbonation resistance of concrete. Beyond these limits, GNP had a negative effect on carbonation. Khan et al. [19] investigated ECC performance with binary or ternary usage of silica fume (SF), metakaolin (MK) and GNP. The optimum mechanical and environmental performances were achieved with 10% cement replacement using SF or MK individually, or with 20% cement replacement using SF and MK equally. In both cases, 0.03% GNP inclusion was reported to enhance the ECC performance. Hang et al. [20] studied the mechanical properties of functionally graded GNP reinforced cement composites with different distribution patterns through experiments and modelling. The flexural strength and peak compressive load of symmetrically graded specimens was higher compared to uniform distributed specimens. The developed model considering the effects of agglomeration and pores, accurately predicted the Young's Modulus and cracking loads, agreed with the experimental data. GNP was also used in studies of self-sensing [21, 22], 3D printing [23, 24], structural health evaluation [25, 26], and modelling [27, 28].

1.1 Motivation, aim and scope

The limited service life, durability issues, and high maintenance costs associated with cementitious composites have led to the exploration of self-healing solutions [29]. Self-healing cementitious composites, such as Engineered Cementitious Composites (ECC), offer a promising approach for addressing these challenges. ECC exhibits autogenous self-healing capabilities, particularly through multiple tight width cracking [30]. However, the influence of Graphene Nanoplatelets (GNP) on the self-healing behavior of cementitious composites is not well-documented. This research aims to investigate the potential impact of GNP on ECC's self-healing properties and compare its effectiveness, given the positive results observed in previous GNP studies on cement-based materials. Besides, GNP was not used in ECC design before in a way that both mechanical and self-healing properties have been studied together. Therefore, the aim of this study is to examine the impacts of GNP inclusion on fresh, mechanical, non-destructive properties and self-healing performance of ECC. The change in mechanical and non-destructive properties and also self-healing behavior of control (named as ECC) and graphene nanoplatelet (named as ECC-G) specimens were observed through different mechanical and nondestructive testing (NDT) methods. The test methods

applied in the study were compressive strength test, four-point bending test, resonant frequency (RF) test, ultrasonic pulse velocity (UPV) test, sorptivity test, electrical impedance (EI) test, microscopic inspection, SEM, EDS and XRD analyses.

2 Experimental method

2.1 Materials and mixture

The main focus of the study is to investigate the effect of Graphene Nanoplatelets on self-healing properties of ECC through mechanical and NDT tests. ECC with and without GNPs were produced by using CEM I 42.5 Portland Cement (PC), Class C fly ash (FA) as binders, fine silica sand (0–200 μm), GNP, water (w), polyvinyl-alcohol (PVA) fibers, and polycarboxylate-ether based high range water-reducing admixture (HRWRA). PVA fibers have a length of 8 mm and a diameter of 40 μm , with a tensile strength of 1600 MPa, and a specific gravity of 1.3. GNPs used in this study have a thickness of 5nm and a diameter of 18 μm and a specific surface area of 170 m^2/g . Table 1 presents the chemical and the physical properties of Portland cement and fly ash. Fig. 1 and Fig. 2 show SEM images of GNP nanoparticles and particle size distribution of fine sand respectively. Table 2 shows the proportions of the ECC mixture.

Table 1 Chemical and physical properties of binders

Chemical composition	PC (%)	Fly ash (%)
CaO	62.90	11.21
SiO ₂	18.62	50.04
Al ₂ O ₃	4.60	22.85
Fe ₂ O ₃	3.57	8.02
MgO	2.76	2.23
Na ₂ O	0.22	0.27
K ₂ O	0.58	2.5
SO ₃	2.71	0.78
Physical properties		
Specific gravity	3.13	2.28
Blaine fineness (cm^2/g)	3150	2850

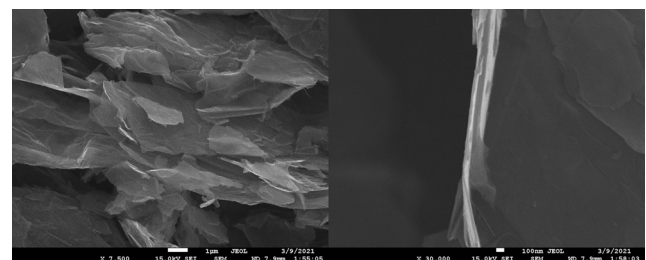


Fig. 1 SEM images of Graphene Nanoplatelets (GNPs)

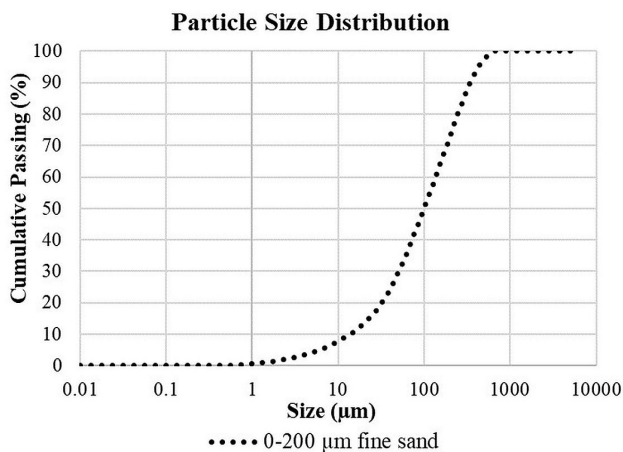


Fig. 2 The particle size distribution of 0–200 µm fine sand

Table 2 The mix proportions of ECC mixture

Materials	kg/m ³					
	PC	FA	Water	Sand	HRWRA	PVA
Proportions	555	666	333	438	7.4	26
Ratio name	GNP/ <i>cm</i>	FA/ PC	<i>w/</i> <i>cm</i>	Sand/ <i>cm</i>	HRWRA/ <i>cm</i>	PVA/ <i>V</i>
Ratio value	0.05	1.2	0.27	0.36	1.3%	2%

cm: cementitious materials, *V*: total volume

2.2 Mixing procedure

The ECC mixture was prepared and mixed in a vertical planetary mixer with a capacity of 20 liters. For the control ECC mixture, all solid ingredients, except fibers (binding materials and sand) were initially combined and mixed until a certain uniformity was achieved among solids. The dry mix was subsequently combined with water and HRWRA until achieving optimal plasticity and satisfactory workability properties.

To assess workability properties, a mini-slump flow test was conducted before and after fiber addition. A conical flow mold described in ASTM C230/C230M-23 [31] with 70 mm-top opening, 100 mm-bottom opening and 50 mm-height was used for the application of mini-slump flow test complying with TS EN 12350-8 [32]. During the test, the flow cone was positioned on a flat, rectangular glass piece and completely filled with ECC mixture. After filling, the cone was removed and the flow diameter was measured as an indicator of flowability and workability. Finally, PVA fibers were added and mixed until an even distribution throughout the matrix was visually observed. Once all the ingredients were mixed and the mixing procedure was completed, the fresh ECC control mix was transferred into the molds to produce the specimens required for mechanical and non-destructive tests.

However, a slightly different procedure was followed for the mixture with GNP in which an ultrasonically treated GNP suspension was used. GNP suspension was prepared by adding and stirring GNP in mixing water along with HRWRA. As it was stated before, since they possess a hydrophobic nature, GNPs tend to agglomerate in water. As a result, uniform GNPs should be stabilized and uniformly dispersed before usage. The combination of ultrasonic treatment, mechanical mixing and surfactants usage has proven to be a widely utilized technique to disperse and stabilize GNPs in cement.

This approach is effective on enhancing the dispersion and stabilization of GNPs in water with the usage of a polycarboxylate-based superplasticizer as a surfactant [33]. Thus, the GNPs were treated in an ultrasonic bath, and polycarboxylate-ether based HRWRA was used as the surfactant. Based on the findings from the literature, the amount of GNP to be used was chosen as 0.05% of the total cementitious materials content, average duration was scheduled as 45 minutes [12, 13, 34] for ultrasonic bath treatment [7, 8, 13], and the amount of polycarboxylate-ether based HRWRA to be used was determined as 10 times of GNP content [34–36]. The rest of the HRWRA amount was added during mixing. The ultrasonic treatment was observed to be effective on achieving the dispersion and the stabilization of GNPs in cementitious matrix and prevented the agglomeration of GNP particles [13]. Fig. 3 presents the comparison between GNP suspensions with and without the subjection of 45-minute ultrasonication in terms of dispersion and stability. The visuals of ultrasonically treated and untreated GNP suspensions after 48 hours and after one week can be found in Fig. 3 as well. In Fig. 3 (c) and Fig. 3 (d), the visuals are presented to emphasize the efficiency of ultrasonic treatment and the preservation of that efficiency over time. It is seen that even though the ultrasonic treatment lost its initial effectiveness slowly over time, the treatment still provided the dispersion and prevented the agglomeration of GNP particles in water in comparison to untreated suspensions. GNP suspension that was ultrasonically treated and additional HRWRA were added to dry constituents immediately after treatment and mixed.

All components were combined and mixed until the mixture became adequately workable. Mini-slump flow test was again conducted on ECC-G mix with and without fiber to control workability properties. Fig. 4 shows an illustration of the fresh ECC-G mixture before and after the addition of PVA fibers following the slump flow

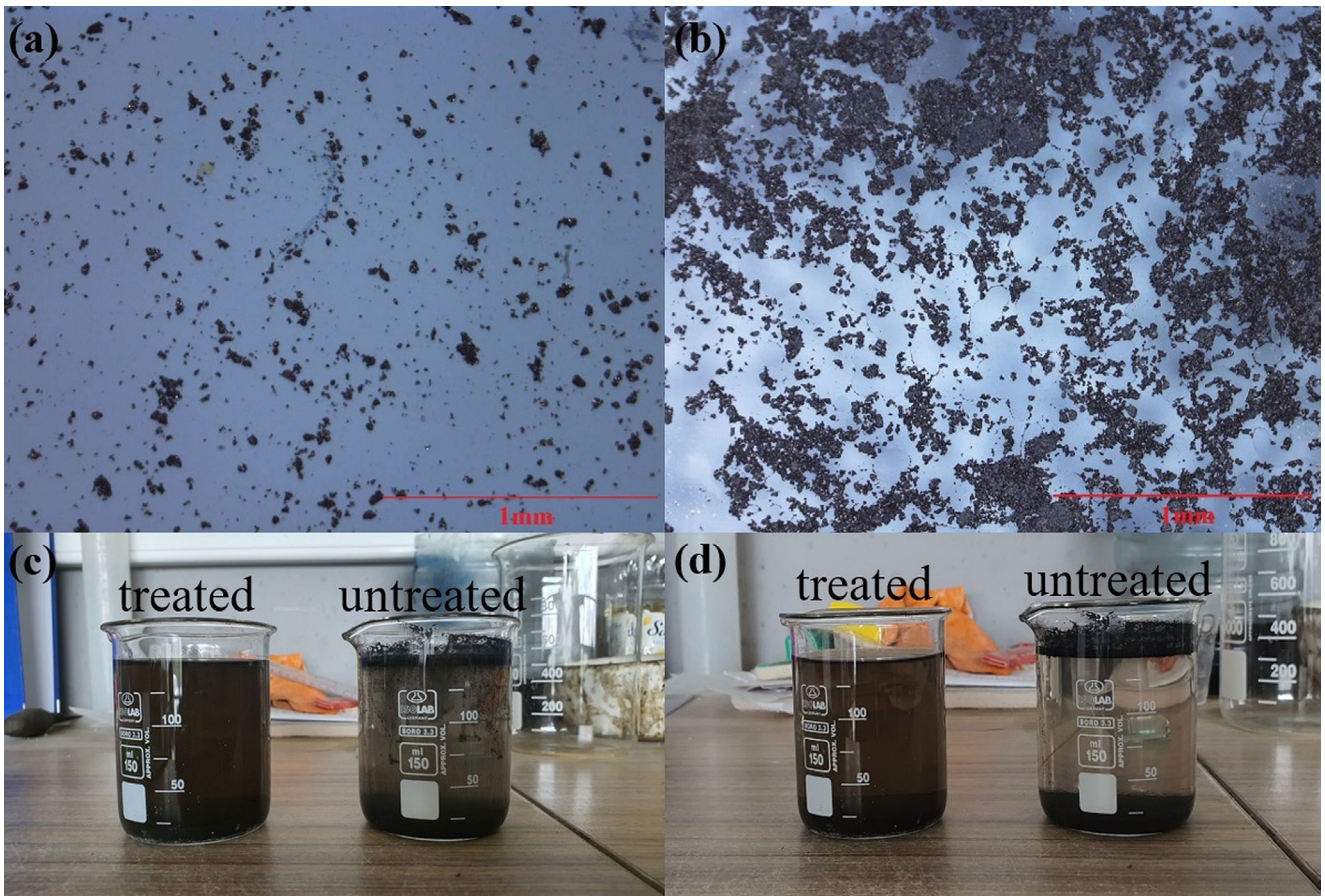


Fig. 3 The dispersion and stability conditions of GNP suspensions (a) with ultrasonic treatment (b) without ultrasonic treatment; the visuals of GNP suspensions (c) after 48 hours, and (d) after 1 week

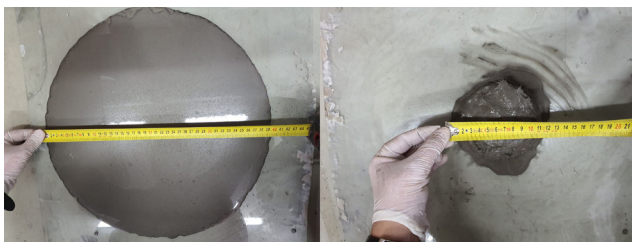


Fig. 4 An example mini-slump flow test before and after fiber addition

test. The amounts of HRWRA for each ECC casting and related slump flow diameters are given in Table 3. Since GNP has a negative effect on the workability due to its hydrophobic nature, agglomeration potential, large specific surface area, high aspect ratio and strong Van der Waals bonds between particles [37, 38], it can be seen that more amount of HRWRA was used to achieve the same level of flowing ability. PVA fibers were finally incorporated and mixed thoroughly to ensure even distribution and avoid bundling throughout the matrix. The fresh ECC-G mix was poured into the molds to produce the specimens for mechanical and non-destructive testing once the mixing operation was completed. Following the mixing, all specimens prepared were left in the molds for a period of

Table 3 The HRWRA amounts and slump flow test results

Mixture	HRWRA (kg/m ³)	Flow without fiber (cm)	Flow with fiber (cm)
ECC	10.5	40	10
ECC-G	14.1	41	10

24 hours. All specimens were removed from the molds after 24 hours and transferred in isolated plastic curing bags to maintain the moisture and support the autogenous curing until the desired testing age.

2.3 Testing procedure

2.3.1 Compression test

The compression test was performed in accordance with ASTM C109-21 [39]. The compressive strengths of cubic specimens for both ECC and ECC-G mixtures were measured at the ages of 7 and 28 days. For each age, three cubic specimens with the dimensions of 5 × 5 × 5 cm were tested with compression test device. Until the day of testing, specimens were stored in plastic bags. On testing day, the specimens were removed from the plastic bags. The cubic specimens were tested using an automatic compression testing machine with a 1.35 kN/s loading rate.

2.3.2 Four-point bending test

Four-point bending tests were applied on beam specimens with the dimensions of $18 \times 7.5 \times 2$ cm by a deformation controlled electromechanical universal testing machine with a setup similar to TS EN 12390-5 [40] as seen in Fig. 5. A loading rate of 0.005 mm/s was adapted in flexural test.

The bending test was employed to determinate the flexural properties and to evaluate self-healing by mechanical means at early and later ages. For this reason, the bending test was conducted at the ages of 7+0 days, 7+14 days and 7+35 days, also at the ages of 28+0 days, 28+14 days and 28+35 days. At each age, six specimens were used for the four-point bending test. The specimens of these ages were separated into three virgin (V) and three preloaded (PL) set specimens. On the 7th and 28th days, the beam specimens were removed from their plastic bags and divided into two groups as virgin and preloaded sets.

Three specimens of the virgin set were first tested with the four-point bending test device up to failure. The specimens in second group were subjected to a preloading process, where they were loaded to a level equivalent to 70–75% of ultimate flexural load sustained by the virgin specimens. This preloading step aimed to introduce controlled damage and create initial cracks in the specimens for the evaluation of the flexural behavior and self-healing performance.

For all preloaded specimens, the crack openings were typically kept around 150 μm . After the PL set specimens of 7+0 and 28+0 days were preloaded, three of the specimens were once again loaded up to failure. The remainders were placed into a water bath at the temperature of 23 ± 2 °C. This immersion in water bath allowed for the occurrence of self-healing processes and continued hydration reactions to take place until specified testing ages.



Fig. 5 The four-point bending setup

Aside from the mechanical tests, several nondestructive tests were also applied to virgin and preloaded ECC mix and ECC-G mix specimens. After PL beam specimens were preloaded at 7 and 28 days, the 7+35 and 28+35 days beam specimens were nondestructively tested with resonant frequency and ultrasonic pulse velocity test methods.

2.3.3 Resonant frequency test

The resonant frequency test, conducted according to ASTM C215-19 [41], was used for observing the changes in the resonant frequency and the dynamic modulus of ECC specimens with and without GNP after preloading and self-healing. Since the natural frequency of vibration or in other words fundamental resonant frequency of a specimen is essentially associated with the dynamic modulus of elasticity and the structural integrity of the specimen [42], it can be used to determine the dynamic modulus. When the cementitious materials are undergoing a deteriorating effect such as preloading or an improving effect such as self-healing, the change in mechanical integrity will lead to an alteration in the resonant frequency. Accordingly, the changes in the dynamic modulus (E) can be detected by monitoring the variations in the resonant frequency (n) since there is a relationship between these parameters as defined in Eq. (1) [41] which also includes mass (M) and dimension coefficient (C) of the specimen.

$$E = CMn^2 \tag{1}$$

For this test, a resonant frequency meter with a maximum sampling frequency of 100 kHz was used. The specimen dimensions and mass were input, and the specimens were subjected to impact at specific locations in transversal and longitudinal vibration modes. The accelerometer was used to detect the vibrations in the specimen, and the frequency values were measured with a frequency meter. The schematics of resonant frequency test can be seen in Fig. 6.

2.3.4 Ultrasonic pulse velocity test

The ultrasonic pulse velocity test was complying with ASTM C597-22 [43]. The UPV test was employed to indicate the changes in pulse velocity and dynamic modulus of

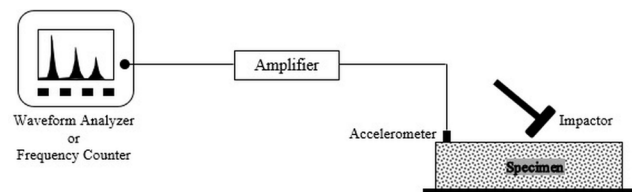


Fig. 6 The resonant frequency test

elasticity under the effect of preloading and self-healing. To include the impact of cracks and to evaluate the effectiveness of self-healing in the preloaded specimens compared to virgin specimens, indirect transmission testing was applied in UPV test. When an ultrasonic pulse passes through concrete and comes across a crack oriented perpendicular to its path, it will undergo diffraction around the crack. As a result, the pulse travel time will be longer, and the pulse velocity will be lower than that of a sound concrete [42]. As the pulse reaches to self-healed crack, the diffraction of the pulse will be less with the effect of self-healing and the pulse velocity will be higher compared to the previous preloaded state. The dynamic elastic modulus (E) of the specimens is influenced by changes in ultrasonic pulse velocity (V), as there exists a correlation between the two parameters. This correlation is given as Eq. (2) in which Poisson's ratio (μ) and density (ρ) of the specimens are included as well [43].

$$V = \sqrt{\frac{E(1-\mu)}{\rho(1+\mu)(1-2\mu)}} \quad (2)$$

In the measurement of UPV, transducers operating at a frequency of 54 kHz and located on the same face with a 12.5 cm distance between them were used through indirect transmission. The transit time was measured electronically with a measuring unit. The pulse velocity was calculated automatically via the main unit by dividing the distance to transit time. The schematics of ultrasonic pulse velocity test is shown in Fig. 7.

Cylindrical specimens were utilized for nondestructive testing as well by cutting them by a diamond saw into puck-shape specimens with $\text{Ø}10 \times 5$ cm dimensions. The puck-shaped PL specimens were subjected to preloading by splitting tensile test and the formation of cracks was visually monitored during the splitting procedure at the ages of 7 and 28 days. The crack openings were around 150 μm . 7+35 and 28+35 days' puck specimens were tested nondestructively using sorptivity and electrical impedance (EI) test methods.

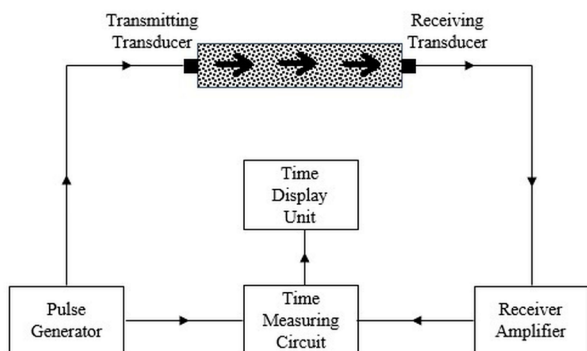


Fig. 7 The ultrasonic pulse velocity test

2.3.5 Sorptivity test

The sorptivity test was applied similar to the procedure described in ASTM C1585-20 [44]. This test method was used to determine the initial rate of water absorption of virgin and preloaded ECC specimens with and without GNP when exposed to water solely from one surface in an unsaturated and sealed condition. The sorptivity test method was employed by subjecting single surface of the oven-dry specimens to water exposure while sealing the other surfaces with rubber tapes. After placing specimens on rod supports in a pan filled with water to a level of about 2 mm above the supports, the change in mass of the specimens was measured for 6 hours.

PL specimens exhibited higher water adsorption rates compared to virgin specimens after preloading. However, the sorptivity of the specimens reduced over time with the effect of self-healing and crack closure. Accordingly, the susceptibility of specimens to water penetration and the effectiveness of self-healing was determined by measuring the increase in mass of specimens in a limited period of time. An example of sorptivity test is shown in Fig. 8.

2.3.6 Electrical impedance test

The electrical impedance test was carried out by using a concrete resistivity meter following ASTM C1876-19 [45]. The EI test allows to calculate the electrical resistance of virgin and preloaded ECC specimens to transfer of ions when subjected to an electrical field in saturated condition. This test also provides an indication about the resistance against the penetration of fluid or aggressive ions. Since electrical resistance is the inverse of electrical conductivity, this test method is comparable to rapid chloride ion penetration test. The PL specimens had lower electrical resistance or impedance compared to virgin specimens after preloading. However, the electrical resistance increases over time with the effect of self-healing and crack closure. The fixed frequency measuring mode

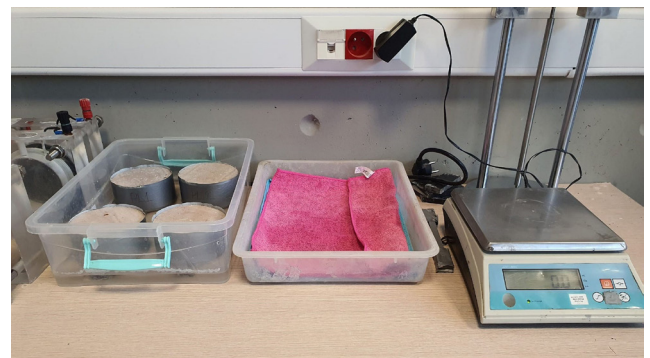


Fig. 8 The sorptivity test

was employed in the EI test. This mode allowed measurements to be taken at 1 kHz fixed frequency. To assess the effect of the crack axis on the results, readings were obtained in directions parallel and perpendicular to the crack direction for PL set specimens. To establish an uninterrupted flow of electrical charge, wet sponges were used between the electrodes and the specimens. An example of electrical impedance test is presented in Fig. 9.

2.3.7 Microscopic inspection

During the microscopic inspection, the crack openings of preloaded specimens with and without GNP at 20× and 200× magnification were recorded and measured using a digital microscope. The measurements of crack closures and the efficiency of self-healing were observed. With the effect of self-healing under water curing, the crack opening values decreased over time. After the first application of each nondestructive test, the specimens were returned to the water bath environment to ensure the process of self-healing and to allow for the continued hydration reactions to take place. This nondestructive testing procedure was repeated weekly until the age of 7+35 and 28+35 days. Table 4 shows the details of specimens used in mechanical and nondestructive tests.

3 Results and discussion

The primary aim of this study is to assess the influence of GNP addition on mechanical properties and self-healing, employing both mechanical and non-destructive tests. Compression and flexural tests, as well as non-destructive tests including resonant frequency, ultrasonic pulse velocity (UPV), sorptivity, and electrical resistivity tests, were conducted for this purpose. To enhance the interpretation of the results obtained from these tests, the evaluation of SEM-EDS and XRD analysis results was found to be beneficial.

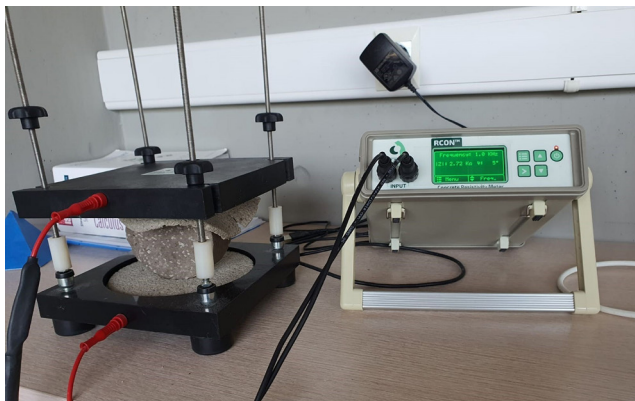


Fig. 9 The electrical impedance test

Table 4 The specimens used in the experimental study

Age (days)	Test
7+0, 7+14, 7+35 28+0, 28+14, 28+35	4-point Bending Test; 6 beam specimens - 180 × 75 × 20 mm (3 virgin + 3 preloaded) (preloading at 7 and 28 days)
7, 28	Compression Test; 3 cubic specimens - 50 × 50 × 50 mm 6 beams - 180 × 75 × 20 mm (3 virgin + 3 preloaded)
7+35 28+35	After preloading at 7 and 28 days, to all specimens in every week; Resonant Frequency Test, Ultrasonic Velocity Test To preloaded specimens; Visual inspection, Self-healing control 3 cylinders = 9 pucks - Ø100 × 50 mm After preloading at 7 and 28 days, in every week;
7+35 28+35	4 pucks - (2 virgin + 2 preloaded) Sorptivity Test 5 pucks - (2 virgin + 3 preloaded) Electrical Impedance Test To preloaded specimens; Visual inspection, Self-healing control

3.1 Microstructural observations

3.1.1 XRD observations

In order to evaluate the effect of GNP on hydration products, X-ray Diffraction (XRD) spectra of control and GNP containing mixtures were obtained by using Copper (Cu) Alpha (K) radiation between 2θ angles of 5–70° by using powder materials scratched from the surface of broken specimens. The superposition of the XRD spectra of control and GNP containing samples is presented in Fig. 10.

After comparing the XRD patterns, it is initially noticeable that the two spectra are largely similar which is in line with the fact that GNP addition does not alter the hydration products rather it improves it by acting as alternative nucleation site and through filling effect. However, ECC-G samples one significant difference is portlandite (P: Ca(OH)₂) peaks which manifest around 2θ of 18 and 34°. Beside the major calcite (C: CaCO₃) peak around

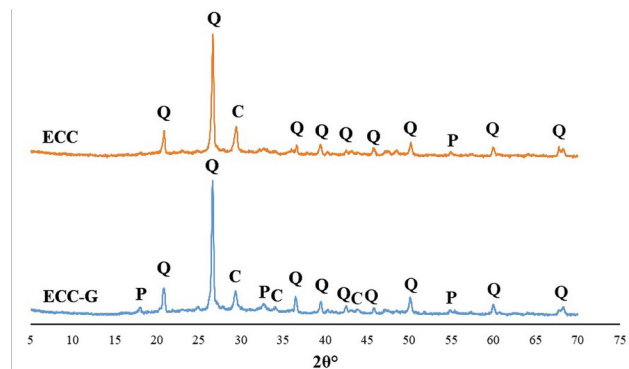


Fig. 10 XRD spectra of ECC and ECC-G samples (Q: SiO₂, P: Ca(OH)₂, C: CaCO₃)

29.5° appears to be less pronounced. This indicates that the carbonation is less in the case of GNP as a result of a more compacted structure preventing the permeation of CO₂ and increasing the carbonation resistance which is also in line with the observations of Zhang et al. [18].

3.1.2 SEM and EDS observations

In order to further understand the contribution of GNP on self-healing mechanism the microstructures of the healed cracks were investigated by Scanning Electron Microscopy

(SEM) analysis along with the Energy Dispersive X-ray spectroscopies (EDS). For SEM analysis, bulk samples with healed crack lines were cut and removed from ECC and ECC-G specimens by a rotary cutter. The SEM images of ECC and ECC-G samples with different magnifications are given in Fig. 11.

Fig. 11 illustrates that the images of ECC-G samples appear significantly clearer and sharper while, the images of ECC samples are more cluttered and charged. These visual differences are the result of the conductive nature of GNPs.

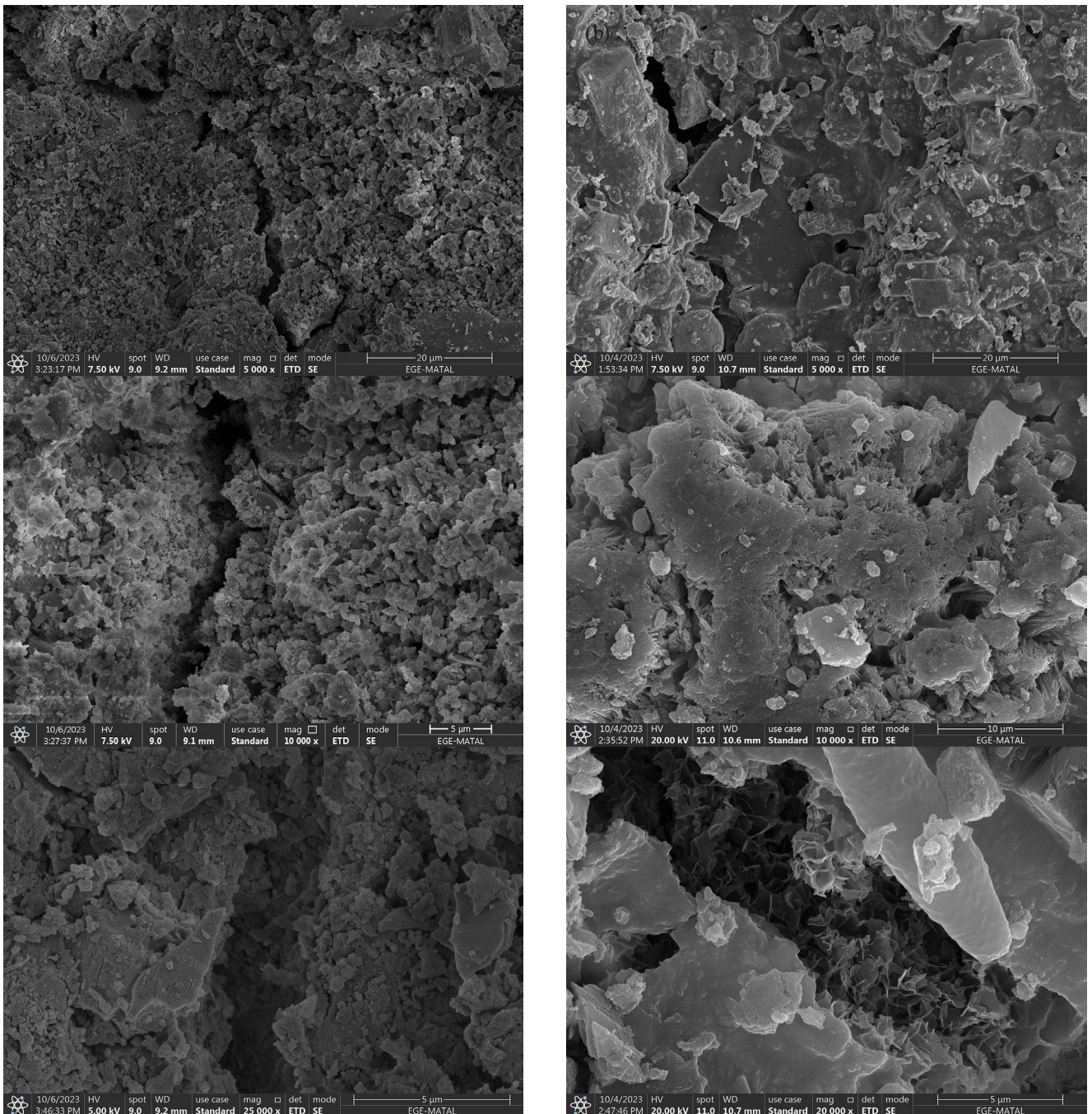


Fig. 11 (a) SEM images of ECC and (b) ECC-G samples

The presence of GNPs in ECC-G specimens promoted the emission of electrons, prevented the electron charging and accordingly provided the improved image clarity. It is also observed that the ECC and ECC-G samples have different microstructures. The microstructure of ECC-G consists of prismatically shaped particles with smooth textures. The microstructure appears more uniform, compact, and interconnected. These observations are consistent with the study of Chen et al. [15]. In contrast, the ECC microstructure is characterized by disorder and irregularity. Its components appear to be detached and discontinuous. The positive effect of GNP mainly arises from the nucleation effect which provides the enhanced and well distributed calcium-silicate-hydrate (C-S-H) gel formation. Although the presence of GNP in the system is evident from the sharper SEM images due to conductive nature of GNP, GNP particles could not be observed individually which may be a consequence of the nucleation effect as hydration products cover the GNP particles upon hydration.

According to the EDS results, in both control and ECC-G mixtures, significant amount of calcium (Ca), silicon (Si) and oxygen (O) are present in the self-healing products. As seen in Fig. 12 and Fig. 13 (a), independent of the GNP inclusion, high Si/Ca ratios were obtained which indicates that the C-S-H gel is the primary healing product in each case. However, in Fig. 13 (b), at some points of measurement, the weight percentage of calcium for ECC-G samples appears to be significantly high compared to ECC samples. The observed low silicon peaks at the same location indicate the formation of CaCO_3 as a self-healing product. As mentioned, in the XRD spectrum of ECC-G samples, portlandite peaks were observed.

Taking this into consideration, it can be suggested that during the self-healing process, portlandite reacts with CO_2 and carbonates inside the cracks.

It can be concluded that GNP containing mixtures produce additional CaCO_3 assisting in filling the crack besides the C-S-H gel observed in control mixtures. Better distribution of hydration products along with the CaCO_3 formation can be considered as the enhanced healing mechanism of GNP containing mixtures.

3.2 Compression test

The cubic specimens were tested under compression in accordance with ASTM C109-21 [39], and the obtained results are presented in Table 5.

Based on the data provided in Table 5, the addition of GNP presented minimal impact on the 7-day compressive strength results. Upon comparing the average compressive strength values of 7-day-old ECC and ECC-G specimens, it is clear that they are nearly identical, indicating that there was no significant increase observed.

In contrast, in 28 days' results, the positive effect becomes more visible. The inclusion of GNP leads to a noticeable increase of 8.64% in the compressive strength values between 28-day-old ECC and ECC-G specimens [7, 8, 10, 14, 16, 36]. This indicates that GNP has a more distinct influence on the compressive strength over a longer curing period. The observed increase in the 28-day values is referred to the filling effect and nucleation effect of GNP [11, 12]. The presence of GNP particles contributes to filling the voids or pores within the cementitious matrix, improving the overall density and compactness. Additionally, GNPs act as nucleation sites for hydration products, promoting

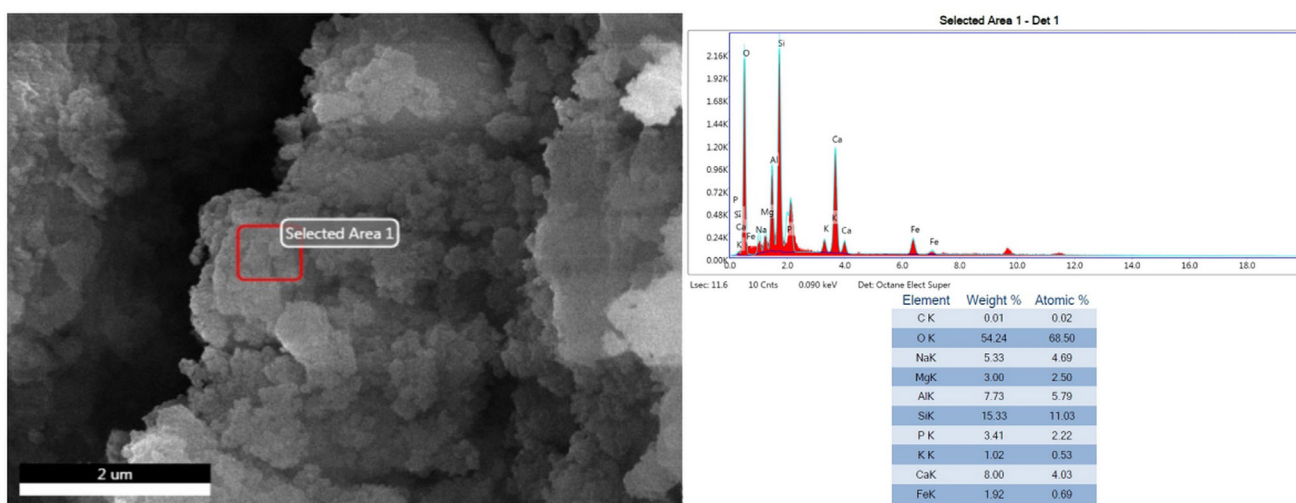


Fig. 12 EDS results of ECC samples

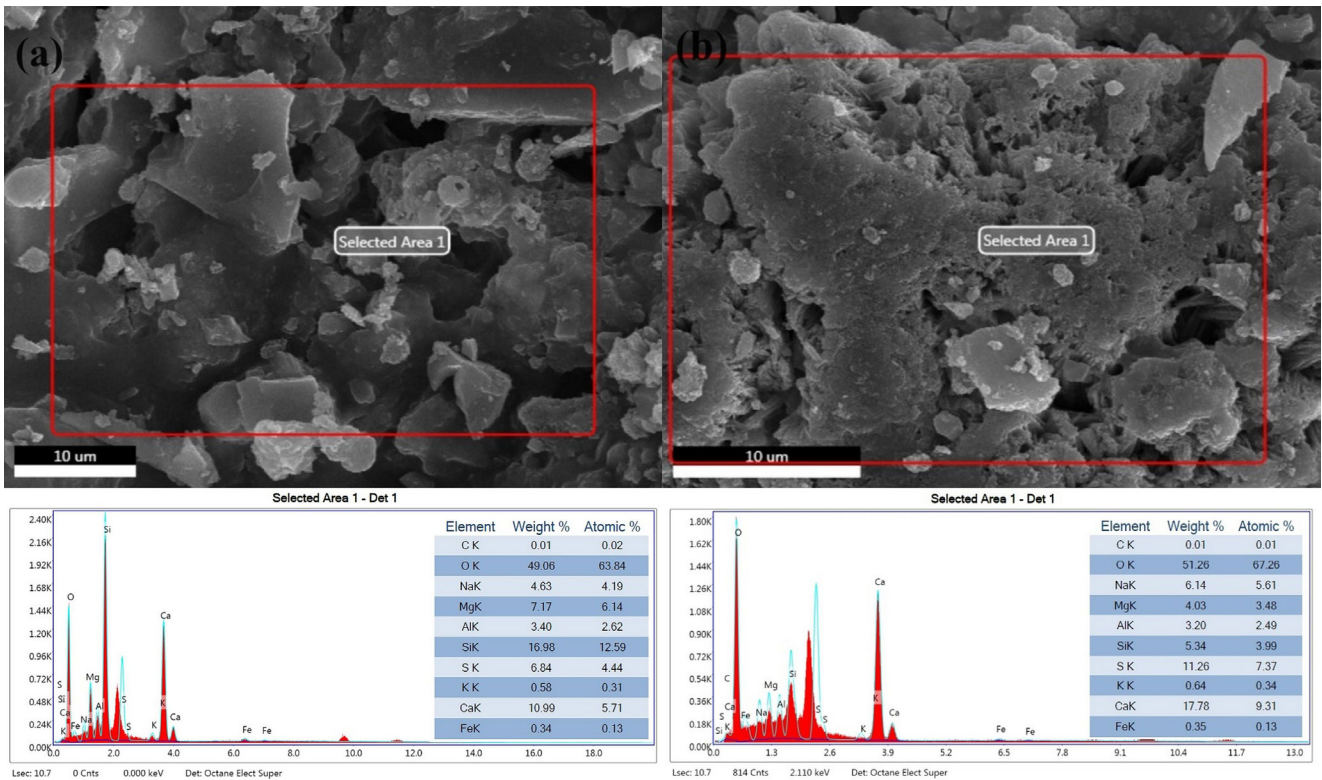


Fig. 13 EDS results of ECC-G samples taken from two different areas: (a) C-S-H gel dominant area (b) CaCO₃ dominant area

Table 5 The compression test results

Specimen type	ECC		ECC-G	
Age	7 days	28 days	7 days	28 days
Comp. Str. (MPa)	52.47	67.16	52.61	72.96
Std. Dev. (MPa)	2.21	0.86	1.22	1.62

Comp. Str.: compressive strength, Std. Dev.: standard deviation

the development of a finer, denser and more interconnected cementitious structure. These combined effects play an important role in enhanced compressive strength of the ECC-G specimens compared to the control ECC specimens. Although there is no consensus on the effect of GNP on the compressive strength. Many studies report increases in compressive strength, while others indicate no significant changes [4, 46]. However, in a study conducted on ECC, a 9% increase in compressive strength was declared, parallel with the increase obtained in this study [19]. The modest rise of the compressive strength can be attributed to the amount and type of GNP incorporated into the mixture. The quantity and inherent characteristics of GNP added to ECC may not be sufficient to produce a substantial improvement in the compressive strength values.

3.3 Four-point bending test

Four-point bending test was conducted on beam specimens with a setup similar to TS EN 12390-5 [40] and the

graphs in Fig. 14; values in Table 6 were obtained. Fig. 14 illustrates the four-point bending performance of ECC and ECC-G specimens.

When the performance of the sound specimens with and without GNP addition are compared, for the specimens loaded at 7 days, a difference of more than 10% occurred between the flexural strengths of GNP and control mixture which consequently reached more than 40% after 35 days additional curing. Similar behavior was also observed in specimens loaded at 28 days with more than 40% increase for both additional curing durations of 14 and 35 days. The increase in deflection capacity is also in favor of GNP containing mixtures as seen in Table 6. The incorporation of GNP resulted in a significant increase in the ultimate flexural strength, first cracking strength, and deformation values for all of the specimens containing GNP as also mentioned in the previous studies [10, 14, 16]. This outcome can be attributed to the micro bridging effect of GNP sheets along with the uniform distribution of hydration products as detailed in microstructural investigation [12, 14, 47].

Addition of GNP significantly altered the overall flexural performance, making it challenging to compare the self-healing behavior of the GNP-added mixture with the control mixture. Substantial drops occurred in both

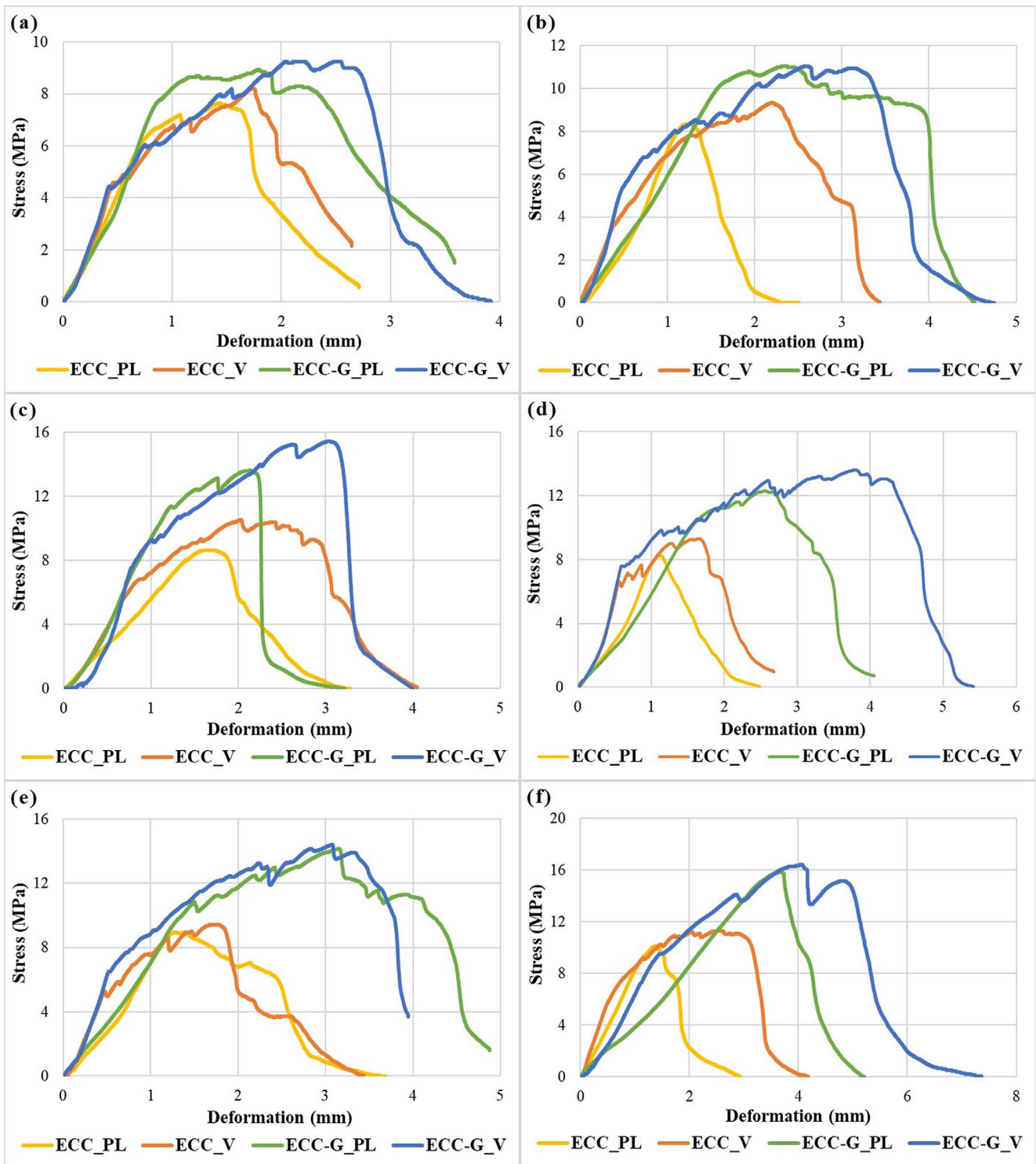


Fig. 14 Four-point bending test results at the ages of (a) 7+0, (b) 7+14 and (c) 7+35 days and at (d) 28+0, (e) 28+14 and (f) 28+35 days

flexural strength and deflection capacities due to preloading. From a mechanical performance standpoint, it can be concluded that none of the damaged specimens with and without GNP could simultaneously reach the strength and deflection capacity of the virgin specimens during the 35-day curing period. However, preloaded ECC-G specimens resulted in closer values to their virgin counterparts

which indicates the contribution of GNP on self-healing. On the other hand, although significant improvements in both strength and deflection capacity were observed in the preloaded specimens, as the contribution of GNP is primarily due to the additional calcite formation along with the improved hydration which would provide additional enhancements, especially in transport properties,

Table 6 The ultimate strength and deformation values

ECC type	Age (days) 7	Specimen type	Ult. Str. (MPa)	Def. at Ult. Str. (mm)	Age (days) 28	Specimen type	Ult. Str. (MPa)	Def. at Ult. Str. (mm)
ECC	+0	PL	7.65 (0.23)	1.42 (0.27)	+0	PL	8.25 (0.72)	1.13 (0.10)
		V	8.20 (0.26)	1.72 (0.12)		V	9.30 (0.42)	1.63 (0.35)
	+14	PL	8.35 (0.47)	1.21 (0.10)	+14	PL	8.95 (0.84)	1.40 (0.30)
		V	9.35 (0.40)	2.18 (0.33)		V	9.42 (0.51)	1.67 (0.20)
	+35	PL	8.65 (0.67)	1.59 (0.16)	+35	PL	10.15 (0.15)	1.40 (0.23)
		V	10.55 (0.27)	2.01 (0.37)		V	11.30 (0.52)	2.50 (0.27)
ECC-G	+0	PL	8.95 (0.22)	1.80 (0.23)	+0	PL	12.30 (0.34)	2.54 (0.30)
		V	9.25 (0.36)	2.50 (0.36)		V	13.60 (0.48)	3.76 (0.33)
	+14	PL	11.05 (0.30)	2.30 (0.17)	+14	PL	14.15 (0.44)	3.14 (0.24)
		V	11.05 (0.62)	2.56 (0.24)		V	14.40 (0.52)	3.06 (0.36)
	+35	PL	13.65 (0.56)	2.13 (0.18)	+35	PL	15.84 (0.21)	3.64 (0.26)
		V	15.45 (0.50)	3.01 (0.50)		V	16.43 (0.16)	4.02 (0.32)

Ult. Str.: ultimate strength value,
 Std. Dev. Values: values in brackets,
 Def. at Ult. Str.: deformation value at ultimate strength

rather than mechanical healing compared to the mixture without GNP. Therefore, complete healing might not be clearly demonstrated through flexural testing within the limited time frame.

3.4 Resonant frequency test results

The results of the resonant frequency test, conducted in accordance with ASTM C215-19 [41], on the beam specimens, can be seen in Fig. 15 and Fig. 16 for transversal and longitudinal modes, respectively. Even though, the resonance frequency results of both modes were different from each other, the equivalent dynamic modulus values were quite similar.

3.4.1 Transversal mode

When cementitious materials undergo an enhancing process, such as self-healing, the change in mechanical integrity is expected to result in an alteration, more specifically an increase in the resonant frequency. Accordingly, the changes in the dynamic modulus can be detected by

monitoring the variations in the resonant frequency. As the dynamic modulus of a specimen is closely linked to its resonant frequency, it can be directly calculated using relevant formulas that include the resonant frequency (ASTM C215-19) [41]. Consequently, the dynamic modulus results exhibit a similar pattern. Fig. 15 presents the measured resonant frequency and calculated dynamic modulus values and their corresponding increase.

The resonant frequency test was applied on a weekly basis after preloading at both 7 and 28 days. The detrimental effect of preloading is immediately visible for both modes and ages as PL specimens displayed significantly lower RF values compared to virgin specimens indicating the effect of cracking on structural integrity and mechanical degradation. According to Fig. 15 and Fig. 16, resonant frequency values were observed to evolve with time, irrespective of whether the specimen remained sound or damaged. In the case of PL specimens, this evolution was notably more rapid during early ages compared to virgin specimens. When assessing the self-healing performance

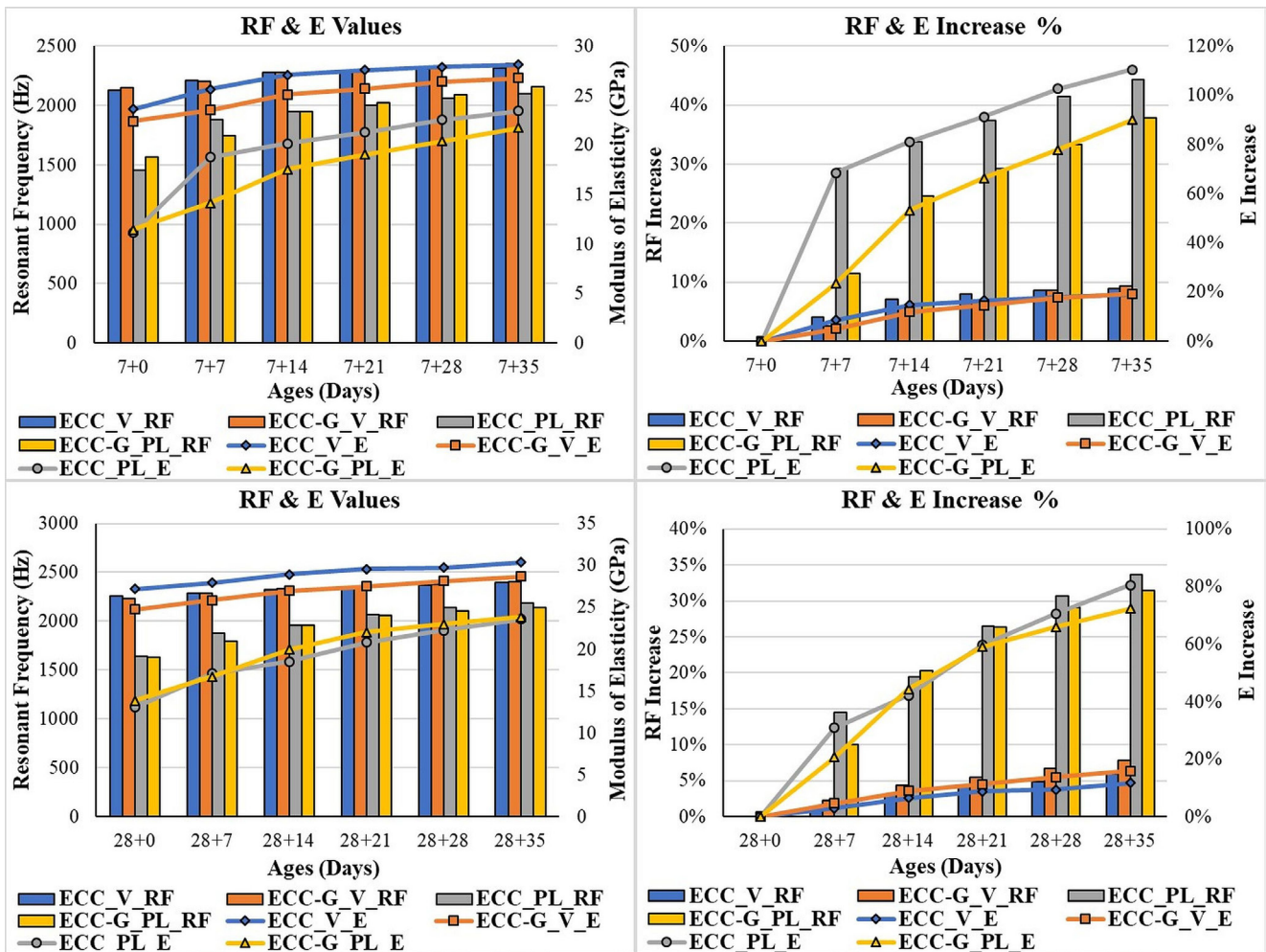


Fig. 15 Resonant frequency test results – RF&E values (7&28 days)

based on RF results, it becomes apparent that damaged specimens exhibit a higher percentage increase in both control and GNP-containing mixtures at both ages. This observation serves as an indicative measure of the self-healing process. However, no significant difference was discerned between the GNP-containing mixture and the control mixture in tests conducted at both 7 and 28 days. The relatively low-frequency values ranging from 1250 to 2500 Hz along with the small specimen dimensions are considered to hinder obtaining measurements with sufficient sensitivity to reveal the effect of self-healing in the transverse mode.

3.4.2 Longitudinal mode

In the longitudinal mode, resonant frequency values ranged from 6900 Hz to 11200 Hz, which is significantly higher compared to the transverse mode, enabling a more sensitive monitoring of the effect of GNP in this mode. Nevertheless, even in the longitudinal mode, resonant frequency values did not indicate a higher dynamic modulus,

despite the positive contribution of GNP addition revealed by mechanical test results. Self-healing is evident for both loading ages, with early age loading at 7 days resulting in a better healing capacity due to the larger quantity of unhydrated binder, providing increased capacity for autogenous healing in the case of early preloading. However, even in the longitudinal mode, it was not possible to distinguish between control and GNP-containing mixtures in terms of self-healing. This outcome aligns with the findings of Zhang et al. (2020) [48], as they concluded that RF may not reflect tensile performance and requires additional performance tests for healing.

3.5 Ultrasonic pulse velocity test results

The ultrasonic pulse velocity test, conducted following the guidelines outlined in ASTM C597-22 [43], on beam specimens as well. The obtained velocity and elastic modulus results are shown in Fig. 17. In UPV test, indirect transmission method was adopted to capture the healing in the cracked zone for PL specimens.

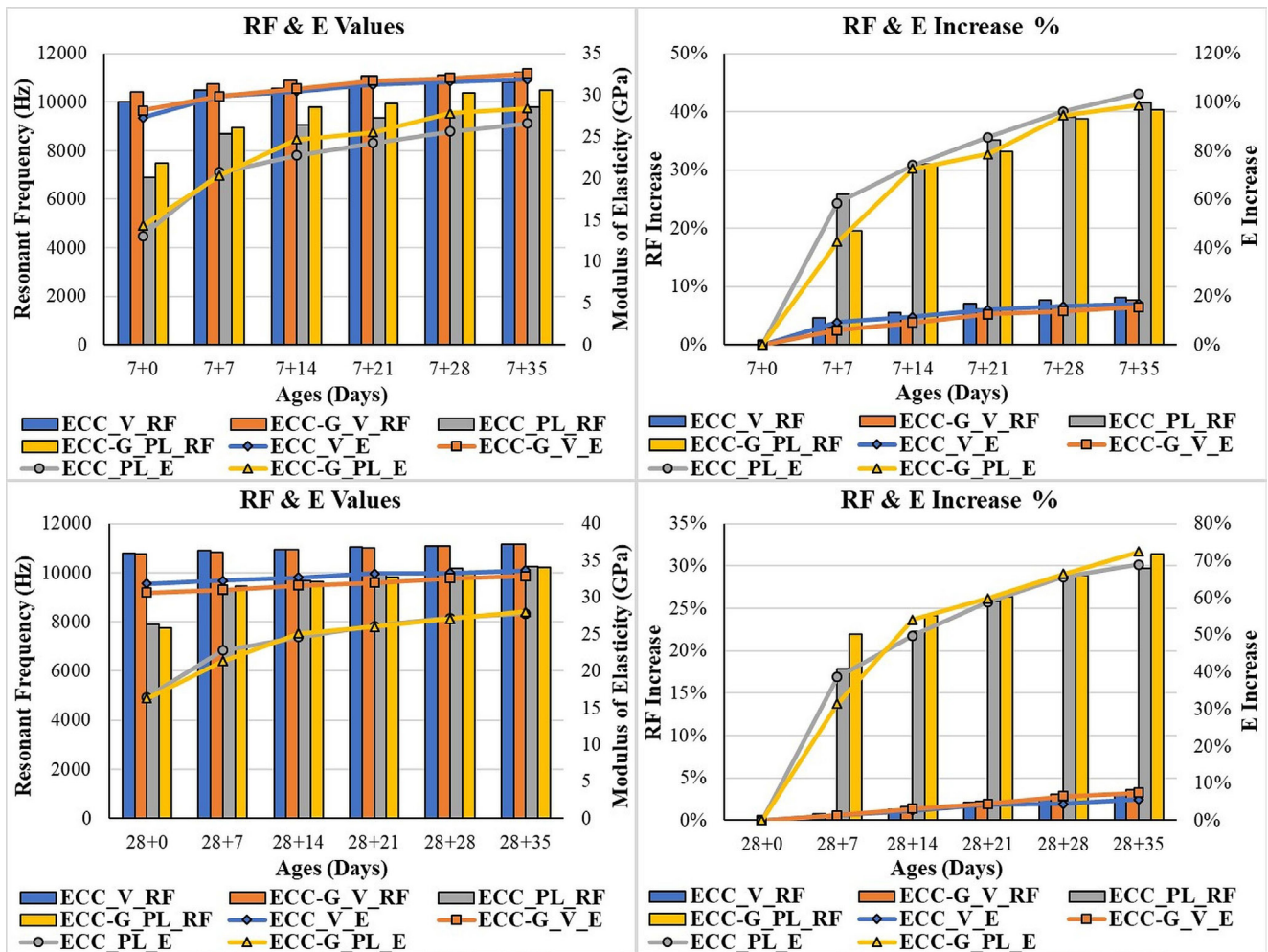


Fig. 16 Resonant Frequency test results – RF&E values (7&28 Days)

The velocity values varied within the range of 4500 and 6000 m/s. According to Fig. 17, the inclusion of GNP had a positive impact on the ultrasonic pulse velocity values of the virgin specimens as a result of pore size refinement attributed to filling and nucleation effects of GNP, especially at early ages. UPV values augmented with time regardless of the GNP addition for both virgin and preloaded specimens as a result of ongoing hydration for virgin specimens while it can be attributed to the shortening of the path as the pulse encounters a self-healed crack or a filled void. In such cases, as the diffraction of the pulse is reduced, higher pulse velocities are obtained compared to the cracked state. Accordingly, the extent of self-healing can be assessed by comparing the increase in UPV (Ultrasonic Pulse Velocity) of preloaded and sound specimens, as the difference arises from the pulse propagation through the healed crack. At the end of 35 days of additional curing, the differences between the UPV values of sound and preloaded specimens of ECC mixture were determined as 13% and 12.5% for preloading ages of 7 and 28 days, respectively. These values clearly

indicate the self-healing capability of the ECC mixture. Besides, the difference between sound and damaged specimens of GNP-containing mixture was calculated as 16.4% and 13.2%, which is considerably higher compared to the ECC mixture. This shows that GNP contributes to self-healing, especially when preloading occurs at an early age. Furthermore, Fig. 18 clearly shows that cracks in the GNP-containing mixture demonstrate enhanced closure in comparison to the control mixture. The microstructural analysis confirmed that the white stain on the cracks, which enables pulse waves to propagate more easily through them, is mostly CaCO_3 . Correspondingly, the equivalent dynamic modulus values presented a similar increase to velocity values based on the relation between pulse velocity and dynamic modulus as defined by ASTM597-22 [43].

3.6 Sorptivity test results

The sorptivity test, in accordance with ASTM C1585-20 [44] was performed on cylindrical puck-shaped specimens and the test results are depicted in Fig. 19 in $\text{mm per min}^{1/2}$.

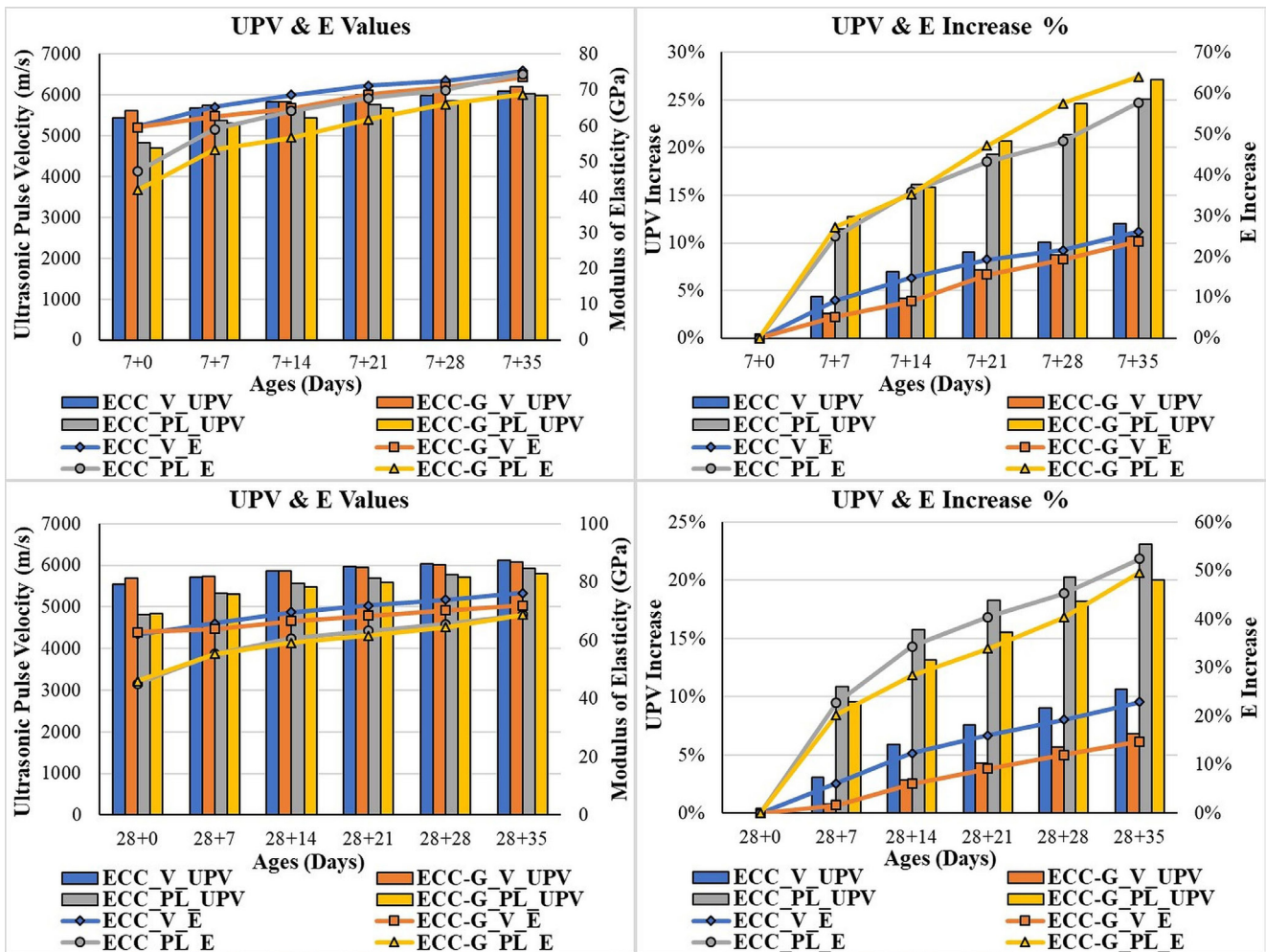


Fig. 17 UPV test results – UPV&E values (7&28 days)

When sorptivity results of the same age specimens in Fig. 19 were considered, it was observed that the water absorption reduction with time was generally greater in specimens with GNP. This indicates that the utilization of GNP particles resulted in a more effective filling effect, leading to the formation of a finer and denser microstructure. The filling effect of the GNP particles played a significant role in achieving a compact and refined matrix where larger pores were subdivided into smaller and finer pores within ECC-G specimens. The results agree with previous research by Lin and Du [11] and Jiang et al. [12] that highlight the filling effect of GNP particles in promoting the production of a denser and more refined microstructure. Since the preloading causes a crack at the surface of the specimen exposed to water, preloading increased sorptivity for both mixtures' preloaded specimens. It is observed that GNP played a crucial role in altering the pore structure, resulting in lower sorptivity coefficients at reference ages of 7 and 28 days. Consequently, the comparison of self-healing capabilities in terms of the sorptivity index

became more challenging. However, for both preloading ages of 7 and 28 days, preloaded specimens of GNP mixtures exhibited a greater reduction in the sorptivity index, especially during the early stages of water curing. As a result, the incorporation of GNP particles not only led to improved water resistance and reduced water absorption but also enhanced the durability and self-healing properties of the ECC-G specimens.

3.7 Electrical impedance test results

Puck-shape cylinders having a thickness of 5 cm were used to determine the electrical resistivity following ASTM C1876-19 [45], and the test results obtained are demonstrated in Fig. 20.

As the test results are dependent on the direction of the current and the crack orientation, for all PL specimens, the cracks were aligned parallel to the direction of the current. Upon comparing the electrical impedance values between ECC and ECC-G specimens of the same age, it becomes evident that the addition of GNP leads

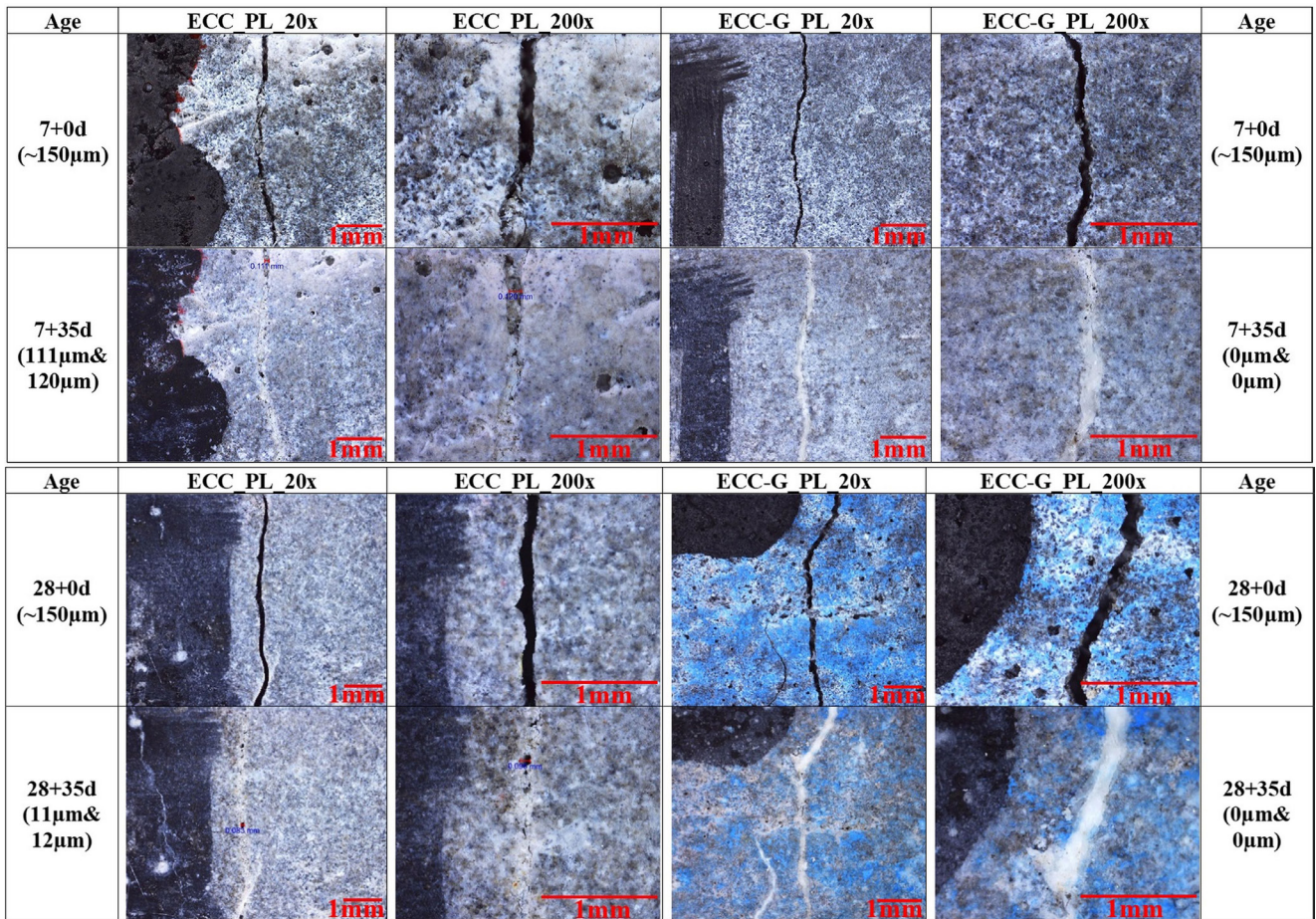


Fig. 18 Microscopic measurements of ECC and ECC-G specimens with 1 mm scale

to an increase in electrical impedance. Specifically, when examining the results of 7 days and 28 days, both the virgin and preloaded ECC-G specimens exhibited higher electrical impedance values compared to the ECC control specimens. This increase in electrical impedance can be attributed to the reduction in interconnected pores resulting from the incorporation of GNP. Since the electrical resistivity is related to the quantity of pores, their connectivity, and the presence of water within them, there was a decrease in interconnected pores, leading to an increase in electrical impedance values with the inclusion of GNP. This relationship highlights the influence of GNP on the electrical properties of the ECC-G specimens by modifying pore characteristics, connectivity and therefore electrical resistivity.

In the case of self-healing, when a crack is filled with self-healing products, electrical current cannot easily propagate, leading to an increase in resistance and, consequently, the impedance of the material. In the case of GNP, calcite is responsible for crack closure. For preloading age of 7 days, the initial impedance values, improvements

in impedance for preloaded and virgin specimens were closely aligned. However, at a loading age of 28 days, significant drops in impedance occurred due to preloading. Although both mixtures exhibited self-healing, the GNP-added mixture gained significantly higher impedance as a result of the healing process. The enhanced self-healing behavior of the GNP specimens enabled them to effectively impede the flow of electrical current in a uniaxial direction resulting in higher electrical impedance values.

Although GNP is a conductive material, it was observed that GNP inclusion increased the electrical impedance results and resistance to electrical current. Since 0.05% is a low GNP concentration, it was commented that the filler effect takes an active part in the electrical impedance results. Therefore, at low GNP concentrations, the GNP addition results in an increase in electrical resistance rather than electrical conductivity. At high GNP contents, the conductive property of GNP plays an important role and causes an increase in electrical conductivity. This behavior was reported by Bai et al. [49] and supports that the electrical properties of GNP are also concentration dependent.

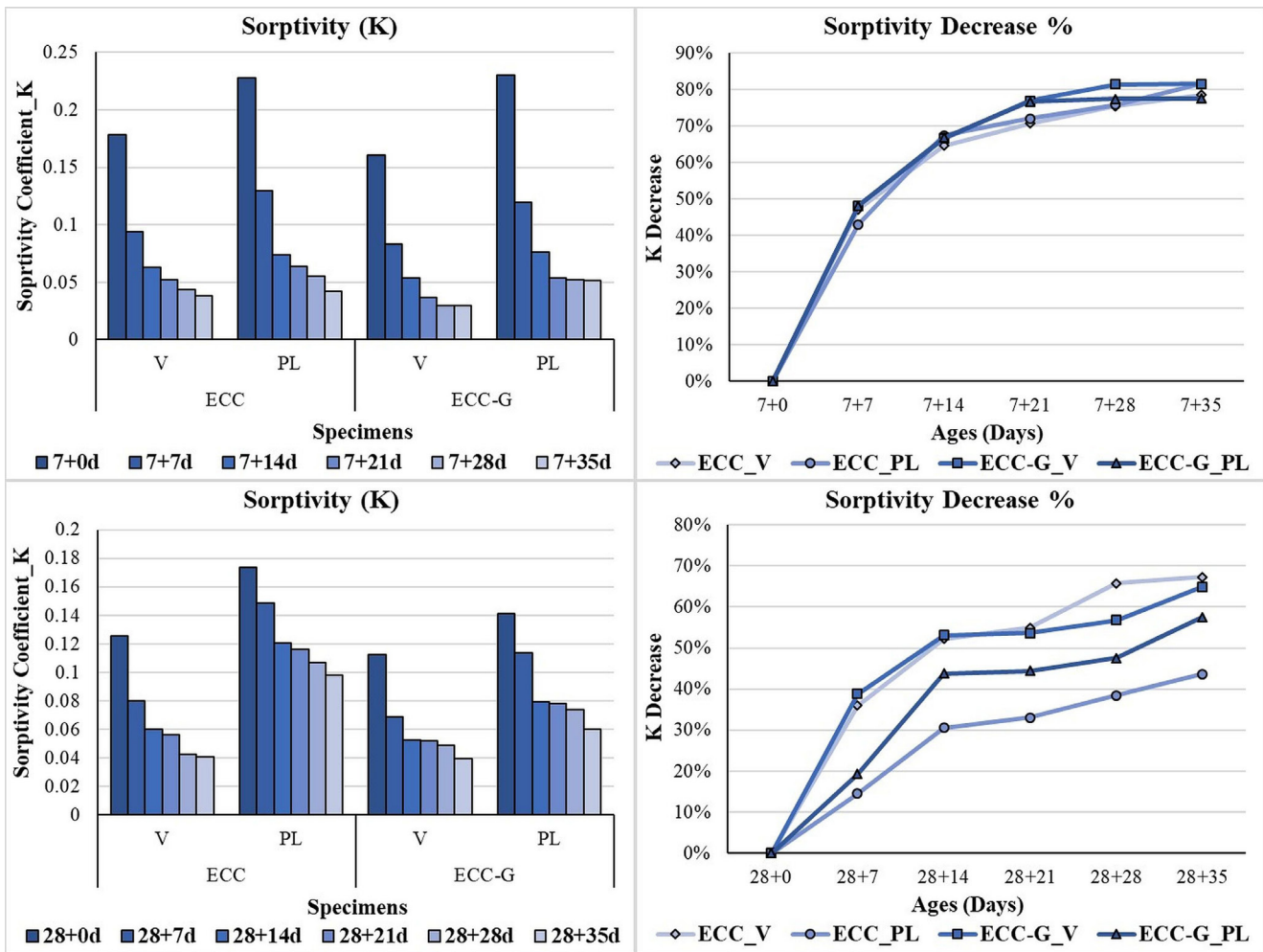


Fig. 19 Sorptivity test results of ECC and ECC-G specimens (7&28 days)

3.8 Microscopic inspection results

Cracks of the beam specimens were subjected to microscopic inspection. The crack images with 1 mm scale in Fig. 18 and crack numbers and openings in Table 7 were obtained.

Based on microscopic inspection results given in Fig. 18, it was seen that ECC specimens showed healing with a decrease in crack opening from 150 μm to roughly 100 μm . When the ECC-G specimens were observed, it became evident that the 150 μm -crack openings had undergone extensive closure, resulting in complete healing within the same period of time in terms of crack closure. As compared to control ECC specimens, the specimens preloaded at 7 days including GNP exhibited self-healing and existing cracks were closed extensively in a period from 7+14 days to 7+35 days. The specimens preloaded at 28 days consisting of GNP were able to self-heal and cracks were closed completely around 28+14 days and remained closed till 28+35 days in comparison with control specimens. Therefore, it can be concluded that the

PL specimens with GNP showed an improved self-healing performance under water curing by comparison with the control specimens and GNP addition positively affected the self-healing behavior of ECC-G specimens. As a result, the addition of GNP improved the flexural performance without compromising, and in some cases, even enhanced the self-healing behavior.

Table 7 indicates that the number of cracks observed in ECC-G specimens after failure is generally higher compared to ECC specimens at various ages of the four-point bending tests. ECC-G specimens outperformed control ECC specimens in terms of strain hardening and multiple cracking. The specimens with GNP displayed enhanced strain hardening and multiple cracking behavior. Additionally, the ECC-G specimens demonstrated higher tensile ductility and energy absorption capacity compared to the control specimens. As Table 7 is inspected in terms of crack opening values after failure, it is seen that the crack opening values of the GNP specimens were typically lower than control specimens. Particularly at the

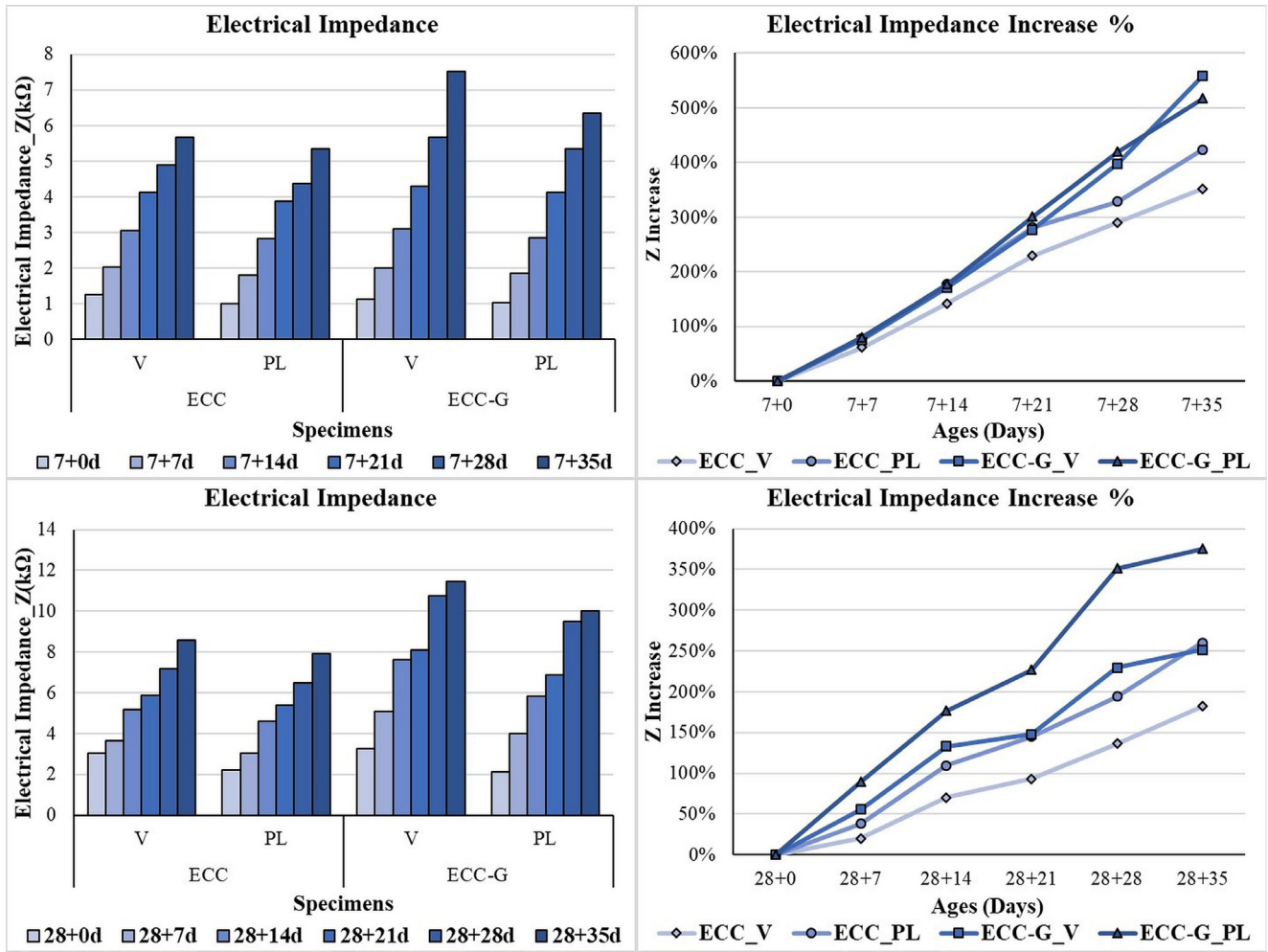


Fig. 20 Electrical Impedance test results of ECC and ECC-G specimens (7&28 days)

Table 7 The crack numbers and openings

Age (days)	After fail.	ECC		ECC-G	
		V	PL	V	PL
7+0	Cr #	4	6	13	10
	ACO	39.5 μm	44.7 μm	42.9 μm	53.2 μm
7+14	Cr #	5	3	13	20
	ACO	48.5 μm	58.7 μm	35.9 μm	37.2 μm
7+35	Cr #	6	2	8	8
	ACO	52.0 μm	112.0 μm	58.9 μm	40.0 μm
28+0	Cr #	5	5	21	18
	ACO	36.4 μm	57.2 μm	40.6 μm	35.6 μm
28+14	Cr #	4	6	16	21
	ACO	40.0 μm	71.5 μm	30.7 μm	41.5 μm
28+35	Cr #	6	1	4	4
	ACO	48.3 μm	27.0 μm	37.2 μm	11.5 μm

Cr #: crack number, ACO: Average Crack Opening

ages of 7+14, 7+35, 28+14, and 28+35 days, the crack openings maintained their tight structure even after the failure. Ultimately, it is commented that GNP affected the crack

formation mechanism and multiple tight opening cracking behavior of ECC-G mix in a positive way according to high crack numbers and low crack opening values. The observed improvements can be the natural results of the GNP bridging effect that hinders the macrocrack formation and the microcrack propagation. This behavior is consistent with previous studies by Jiang et al. [12], Wang and Shuang [14] and Wang and Pang [47].

4 Possible self-healing mechanism

The results obtained from the compression test, four-point bending test, various non-destructive test methods, microscopic inspection, microstructural observations collectively revealed that in addition to compressive strength increment, GNP had a clear improving effect on the flexural behavior, positive contribution to non-destructive properties and a promoting impact on the self-healing. The positive effect of GNP on ECC's self-healing was evident, especially in terms of flexural properties, electrical impedance, microscopic inspection and SEM and EDS

analyses. SEM images showed that GNP inclusion led to a more homogeneous microstructure with more compact and uniformly distributed hydration and self-healing products. These changes are thought to occur with the help of nucleation and filling effects [11, 12], resulting the aforementioned property improvements in ECC. Subsequently, ECC-G specimens exhibited a notable enhancement in self-healing behavior compared to control specimens which can be associated with an improving or promoting effect of GNPs on the existing autogenous self-healing. SEM images and EDS analysis results provided the fact that the self-healing first occurred with the formation of C-S-H gel. However, the formation of CaCO_3 resulted from the carbonation of portlandite in GNP specimens contributed the self-healing as well. Together, these mechanisms promote the self-healing behavior, improve the recovery and the restoration of structural integrity and as well as enhance the mechanical and durability properties.

5 Conclusions

This study examined the influence of GNP on the properties of ECC specimens. GNP was incorporated into the mixtures through an ultrasonically treated suspension prepared with

GNP, water, and a surfactant. The modifications in fresh, mechanical, non-destructive, and self-healing behavior due to 0.05% GNP addition were investigated using mechanical tests, nondestructive tests, and microstructural analyses. In the fresh state, using GNP required the use of a higher dosage of water-reducing admixture to obtain a mixture with flow characteristics similar to the control mixture. For all other tested parameters, the beneficial impact of GNP was evident. Regarding self-healing, positive effects of GNP were clearly observed particularly in terms of mechanical properties, electrical resistivity, and visual inspection. These improvements can be attributed to the more compact and homogeneous structure achieved through GNP addition, as observed in SEM images. The EDS analysis indicated the presence of C-S-H gel as a major self-healing product for both control and GNP containing mixtures. However, it was observed from the XRD results that the samples containing GNP had a higher portlandite content which were converted to CaCO_3 inside the cracks and further enhance the self-healing. It can be concluded that GNP is a promising nanomaterial to be utilized in the enhancement of flexural, nondestructive and more importantly self-healing properties of cementitious composites.

References

- [1] Li, V. C. "Engineered Cementitious Composites (ECC) Material, Structural, and Durability Performance", In: Nawy, E. G. (ed.) Concrete Construction Engineering Handbook, CRC Press, 2008, pp. 24-1–24-46. ISBN 9780429127243
- [2] Li, V. C. "On Engineered Cementitious Composites (ECC): A Review of the Material and Its Applications", Journal of Advanced Concrete Technology, 1(3), pp. 215–230, 2003. <https://doi.org/10.3151/jact.1.215>
- [3] Yang, E. H., Wang, S., Yang, Y., Li, V. C. "Fiber-bridging constitutive law of engineered cementitious composites", Journal of Advanced Concrete Technology, 6(1), pp. 181–193, 2008. <https://doi.org/10.3151/jact.6.181>
- [4] Du, H., Pang, S. D. "Enhancement of barrier properties of cement mortar with graphene nanoplatelet", Cement and Concrete Research, 76, pp. 10–19, 2015. <https://doi.org/10.1016/j.cemconres.2015.05.007>
- [5] Anwar, A., Mohammed, B. S., Wahab, M. A., Liew, M. S. "Enhanced properties of cementitious composite tailored with graphene oxide nanomaterial - A review", Developments in the Built Environment, 1, 100002, 2020. <https://doi.org/10.1016/j.dibe.2019.100002>
- [6] Nanografi "Graphene Nanoplatelets" [online] Available at: <https://nanografi.com/graphene/graphene-nanoplatelets/> [Accessed: 26 June 2023]
- [7] Liu, Q., Xu, Q., Yu, Q., Gao, R., Tong, T. "Experimental investigation on mechanical and piezoresistive properties of cementitious materials containing graphene and graphene oxide nanoplatelets", Construction and Building Materials, 127, pp. 565–576, 2016. <https://doi.org/10.1016/j.conbuildmat.2016.10.024>
- [8] Tong, T., Fan, Z., Liu, Q., Wang, S., Tan, S., Yu, Q. "Investigation of the effects of graphene and graphene oxide nanoplatelets on the micro- and macro-properties of cementitious materials", Construction and Building Materials, 106, pp. 102–114, 2016. <https://doi.org/10.1016/j.conbuildmat.2015.12.092>
- [9] Zheng, Q., Han, B., Cui, X., Yu, X., Ou, J. "Graphene-engineered cementitious composites: Small makes a big impact", Nanomaterials and Nanotechnology, 7, pp. 1–18, 2017. <https://doi.org/10.1177/1847980417742304>
- [10] Tao, J., Wang, X., Wang, Z., Zeng, Q. "Graphene nanoplatelets as an effective additive to tune the microstructures and piezoresistive properties of cement-based composites", Construction and Building Materials, 209, pp. 665–678, 2019. <https://doi.org/10.1016/j.conbuildmat.2019.03.173>
- [11] Lin, Y., Du, H. "Graphene reinforced cement composites: A review", Construction and Building Materials, 265, 120312, 2020. <https://doi.org/10.1016/j.conbuildmat.2020.120312>

- [12] Jiang, Z., Sevim, O., Ozbulut, O. E. "Mechanical properties of graphene nanoplatelets-reinforced concrete prepared with different dispersion techniques", *Construction and Building Materials*, 303, 124472, 2021.
<https://doi.org/10.1016/j.conbuildmat.2021.124472>
- [13] Papanikolaou, I., Ribeiro de Souza, L., Litina, C., Al-Tabbaa, A. "Investigation of the dispersion of multi-layer graphene nanoplatelets in cement composites using different superplasticiser treatments", *Construction and Building Materials*, 293, 123543, 2021.
<https://doi.org/10.1016/j.conbuildmat.2021.123543>
- [14] Wang, B., Shuang, D. "Effect of graphene nanoplatelets on the properties, pore structure and microstructure of cement composites", *Materials Express*, 8(5), pp. 407–416, 2018.
<https://doi.org/10.1166/mex.2018.1447>
- [15] Chen, G., Yang, M., Xu, L., Zhang, Y., Wang, Y. "Graphene Nanoplatelets Impact on Concrete in Improving Freeze-Thaw Resistance", *Applied Sciences*, 9(17), 3582, 2019.
<https://doi.org/10.3390/app9173582>
- [16] Baomin, W., Shuang, D. "Effect and mechanism of graphene nanoplatelets on hydration reaction, mechanical properties and microstructure of cement composites", *Construction and Building Materials*, 228, 116720, 2019.
<https://doi.org/10.1016/j.conbuildmat.2019.116720>
- [17] Zhang, Y., Cui, M., Chen, G., Han, W. "Experimental study of the effects of graphene nanoplatelets on microstructure and compressive properties of concrete under chloride ion corrosion", *Construction and Building Materials*, 360, 129564, 2022.
<https://doi.org/10.1016/j.conbuildmat.2022.129564>
- [18] Zhang, Y., Wang, Y., Yang, M., Wang, H., Chen, G., Zheng, S. "Effect of Graphene Nanoplatelet on the Carbonation Depth of Concrete under Changing Climate Conditions", *Applied Sciences*, 11(19), 9265, 2021.
<https://doi.org/10.3390/app11199265>
- [19] Khan, M. B., Khan, M. I., Shafiq, N., Abbas, Y. M., Imran, M., Fares, G., Khatib, J. M. "Enhancing the mechanical and environmental performance of engineered cementitious composite with metakaolin, silica fume, and graphene nanoplatelets", *Construction and Building Materials*, 404, 133187, 2023.
<https://doi.org/10.1016/j.conbuildmat.2023.133187>
- [20] Hang, Z., Fan, Y., Yang, J., Feng, C., Yang, J., Wang, S. "Improved compressive and flexural performances of functionally graded graphene nanoplatelet reinforced cement composites: Experiments and modelling", *Construction and Building Materials*, 391, 131828, 2023.
<https://doi.org/10.1016/j.conbuildmat.2023.131828>
- [21] Ozbulut, O. E., Jiang, Z., Harris, D. K. "Exploring scalable fabrication of self-sensing cementitious composites with graphene nanoplatelets", *Smart Materials and Structures*, 27(11), 115029, 2018.
<https://doi.org/10.1088/1361-665X/aae623>
- [22] Sevim, O., Jiang, Z., Ozbulut, O. E. "Effects of graphene nanoplatelets type on self-sensing properties of cement mortar composites", *Construction and Building Materials*, 359, 129488, 2022.
<https://doi.org/10.1016/j.conbuildmat.2022.129488>
- [23] Kilic, U., Jiang, Z., Ma, J., Ozbulut, O. E. "Printability characterization of graphene-reinforced cementitious composites", In: Harne, R. L. (ed.) *Behavior and Mechanics of Multifunctional Materials XV: Proceeding of SPIE 11589*, 2021, 1158904. ISBN 9781510640078
<https://doi.org/10.1117/12.2585595>
- [24] Dulaj, A., Salet, T. A. M., Lucas, S. S. "Mechanical properties and self-sensing ability of graphene-mortar compositions with different water content for 3D printing applications", *Materials Today: Proceedings*, 70, pp. 412–417, 2022.
<https://doi.org/10.1016/j.matpr.2022.09.278>
- [25] Le, J.-L., Du, H., Pang, S. D. "Use of 2-D Graphene Nanoplatelets (GNP) in cement composites for structural health evaluation", *Composites Part B: Engineering*, 67, pp. 555–563, 2014.
<https://doi.org/10.1016/j.compositesb.2014.08.005>
- [26] Wang, Y., Zhang, L. "Development of self-sensing cementitious composite incorporating hybrid graphene nanoplates and carbon nanotubes for structural health monitoring", *Sensors and Actuators A: Physical*, 336, 113367, 2022.
<https://doi.org/10.1016/j.sna.2022.113367>
- [27] Fan, Y., Ni, Z., Mu, S., Hang, Z., Wang, Y., Feng, C., Su, Y., Weng, G. J. "Hybrid micromechanical modelling and experiments on electrical conductivity of graphene reinforced porous and saturated cement composites", *Cement and Concrete Composites*, 141, 105148, 2023.
<https://doi.org/10.1016/j.cemconcomp.2023.105148>
- [28] Fan, Y., Yang, J., Ni, Z., Hang, Z., Feng, C., Yang, J., Su, Y., Weng, G. J. "A two-step homogenization micromechanical model for strain-sensing of graphene reinforced porous cement composites", *Journal of Building Engineering*, 71, 106546, 2023.
<https://doi.org/10.1016/j.job.2023.106546>
- [29] Keskin, S. B., Kasap Keskin, O., Anil, O., Şahmaran, M., Alyousif, A., Lachemi, M., Amleh, L., Ashour, A. F. "Self-healing capability of large-scale engineered cementitious composites beams", *Composites Part B: Engineering*, 101, pp. 1–13, 2016.
<https://doi.org/10.1016/j.compositesb.2016.06.073>
- [30] Şahmaran, M., Yildirim, G., Hasiloglu Aras, G., Keskin, S. B., Kasap Keskin, O., Lachemi, M. "Self-healing of cementitious composites to reduce high CO₂ emissions", *ACI Materials Journal*, 114(1), pp. 93–104, 2017.
<https://doi.org/10.14359/51689484>
- [31] The American Society for Testing and Materials "ASTM C230/C230M-23 Standard Specification for Flow Table for Use in Tests of Hydraulic Cement", ASTM International, USA, 2020.
https://doi.org/10.1520/C0230_C0230M-23
- [32] Turkish Standards Institution "TS EN 12350-8: 2019. Testing fresh concrete - Part 8: Self-compacting concrete - Slump-flow test", Turkish Standards Institution, Ankara, 2019.
- [33] Wang, Q., Zhan, D. F., Qi, G. D., Wang, Y., Zheng, H. Y. "Impact of the microstructure of polycarboxylate superplasticizers on the dispersion of graphene", *New Carbon Materials*, 35(5), pp. 547–558, 2020.
[https://doi.org/10.1016/S1872-5805\(20\)60508-X](https://doi.org/10.1016/S1872-5805(20)60508-X)
- [34] Du, H., Pang, S. D. "Dispersion and stability of graphene nanoplatelet in water and its influence on cement composites", *Construction and Building Materials*, 167, pp. 403–413, 2018.
<https://doi.org/10.1016/j.conbuildmat.2018.02.046>
- [35] Metaxa, Z. S., Kourkoulis, S. K. "Dispersion of graphene nanoplatelets reinforcing type II cement paste", *Procedia Structural Integrity*, 13, pp. 2011–2016, 2018.
<https://doi.org/10.1016/j.prostr.2018.12.215>
- [36] Wang, B., Jiang, R., Wu, Z. "Investigation of the Mechanical Properties and Microstructure of Graphene Nanoplatelet-Cement Composite", *Nanomaterials*, 6(11), 200, 2016.
<https://doi.org/10.3390/nano6110200>

- [37] Ge, Z., Qin, J., Sun, R., Guan, Y., Zhang, H., Wang, Z. "The Effect of the Addition of Graphene Nanoplatelets on the Selected Properties of Cementitious Composites", *Frontiers in Built Environment*, 7, 673346, 2021.
<https://doi.org/10.3389/fbuil.2021.673346>
- [38] Jaramillo, L. J., Kalfat, R. "Fresh and hardened performance of concrete enhanced with graphene nanoplatelets (GNPs)", *Journal of Building Engineering*, 75, 106945, 2023.
<https://doi.org/10.1016/j.jobe.2023.106945>
- [39] The American Society for Testing and Materials "ASTM C109/C109M-20 Standard test method for compressive strength of hydraulic cement mortars (Using 2-in. or [50 mm] Cube Specimens)", ASTM International, USA, 2021.
https://doi.org/10.1520/C0109_C0109M-21
- [40] Turkish Standards Institution "TS EN 12390-5: 2019. Testing Hardened Concrete – Part 5. Flexural Strength of Test Specimens", Turkish Standards Institution, Ankara, 2019.
- [41] The American Society for Testing and Materials "ASTM C215-19 Standard Test Method for Fundamental Transverse, Longitudinal, and Torsional Resonant Frequencies of Concrete Specimens", ASTM International, USA, 2019.
<https://doi.org/10.1520/C0215-19>
- [42] Malhotra, V. M., Carino, N. J. "Handbook on Nondestructive Testing of Concrete", CRC Press, 2003. ISBN 9780429191213
<https://doi.org/10.1201/9781420040050>
- [43] The American Society for Testing and Materials "ASTM C597-22 Standard Test Method for Pulse Velocity Through Concrete", ASTM International, USA, 2022.
<https://doi.org/10.1520/C0597-22>
- [44] The American Society for Testing and Materials "ASTM C1585-20 Standard Test Method for Measurement of Rate of Absorption of Water by Hydraulic-Cement Concretes", ASTM International, USA, 2020.
<https://doi.org/10.1520/C1585-20>
- [45] The American Society for Testing and Materials "ASTM C1876-19 Standard Test Method for Bulk Electrical Resistivity or Bulk Conductivity of Concrete", ASTM International, USA, 2019.
<https://doi.org/10.1520/C1876-19>
- [46] Du, H., Gao, H. J., Pang, S. D. "Improvement in concrete resistance against water and chloride ingress by adding graphene nanoplatelet", *Cement and Concrete Research*, 83, pp. 114–123, 2016.
<https://doi.org/10.1016/j.cemconres.2016.02.005>
- [47] Wang, B., Pang, B. "Mechanical property and toughening mechanism of water reducing agents modified graphene nanoplatelets reinforced cement composites", *Construction and Building Materials*, 226, pp. 699–711, 2019.
<https://doi.org/10.1016/j.conbuildmat.2019.07.229>
- [48] Zhang, D., Wu, H., Li, V. C., Ellis, B. R. "Autogenous healing of Engineered Cementitious Composites (ECC) based on MgO-fly ash binary system activated by carbonation curing", *Construction and Building Materials*, 238, 117672, 2020.
<https://doi.org/10.1016/j.conbuildmat.2019.117672>
- [49] Bai, S., Jiang, L., Jiang, Y., Jin, M., Jiang, S., Tao, D. "Research on electrical conductivity of graphene/cement composites", *Advances in Cement Research*, 32(2), pp. 45–52, 2020.
<https://doi.org/10.1680/jadcr.16.00170>